

Stimuli-induced non-equilibrium phase transitions in polyelectrolyte-surfactant complex coacervates

Chloé Seyrig,^a Patrick Le Griel,^a N. Cowieson,^b J. Perez,^c Niki Baccile^{a,*}

^a Sorbonne Université, Centre National de la Recherche Scientifique, Laboratoire de Chimie de la Matière Condensée de Paris, LCMCP, F-75005 Paris, France

^b Diamond Light Source Ltd, Harwell Science and Innovation Campus, Didcot, OX11 0QX, U.K.

^c SWING, Synchrotron Soleil, BP 48, 91192 Gif-sur-Yvette, France

* Corresponding author: niki.baccile@sorbonne-universite.fr

Abstract

Polyelectrolyte-surfactant complexes (PESCs) are important soft colloids with applications in the field of personal care, cosmetics, pharmaceuticals and much else. If their phase diagrams have long been studied under pseudo-equilibrium conditions, and often inside the micellar or vesicular regions, understanding the effect of non-equilibrium conditions, applied at phase boundaries, on the structure of PESCs generates an increasing interest. In this work we cross the micelle-vesicle and micelle-fiber phase boundaries in an isocompositional surfactant-polyelectrolyte aqueous system through a continuous and rapid variation of pH. We employ two microbial glycolipid biosurfactants in the presence of polyamines, both systems being characterized by their responsiveness to pH. We show that complex coacervates (*Co*) are always formed in the micellar region of both glycolipids' phase diagram and that their phase behaviour drives the PESCs stability and structure. However, for glycolipid forming single-wall vesicles, we observe an isostructural and isodimensional transition between complex coacervates and a multilamellar walls vesicle (*MLWV*) phase. For the fiber-forming glycolipid, on the contrary, the complex coacervate disassembles into free polyelectrolyte coexisting with the equilibrium fiber phase. Last but not least, this work also demonstrates the use of microbial glycolipid biosurfactants in the development of sustainable PESCs.

Keywords. Polyelectrolyte-Surfactant Complex (PESC), complex coacervates, biosurfactants, polyelectrolytes, multilamellar walls vesicles

Introduction

Polyelectrolyte-surfactant complexes (PESCs) are a wide class of colloidal systems where surfactant's self-assembly is combined to the complexation properties of polyelectrolytes.^{1–7} In the past three decades a large number of works has shown the interest of a wide community of scientists towards these systems for the broad set of applications in food science,⁸ tissue engineering,⁹ drug and gene delivery,^{2,10} underwater adhesives conception,¹¹ structuring agents,¹² water treatment,¹³ but also personal care, cosmetics,¹⁴ food, pharmaceutical science^{15–17} and much other.^{5–7}

The structure of PESCs depend on many parameters, including the intrinsic packing parameter of the surfactant,¹⁸ rigidity of the polyelectrolyte, charge density and distribution on both surfactant and polyelectrolyte, ionic strength and pH, just to cite the main parameters.^{3,4,6,7,19,20} Supramicellar aggregates are the most common structures when the surfactant is in the micellar region of its phase diagram. They can be found as polyelectrolyte-coated dense aggregates of spheroidal micelles, which can undergo either a solid-liquid,^{3,7} or liquid-liquid,^{3,21} phase separation. In the latter case, they are referred to as complex coacervates.²¹ Supramicellar colloids can also be found in the form of pearl-necklace or cylindrical morphologies.^{3,4} The micellar morphology and structure are generally not affected by complexation,^{3,7,21,22} however, phase transitions can occur inside the supramicellar complexes due to the local rise in concentration.^{3,4,7,23} Multilamellar PESCs, of both flat or vesicular morphologies, have also been explored from a fundamental point of view^{3,5,7,19,24} for their interest in gene delivery applications, as described for DNA-complexed phospholipids, known as lipoplexes.^{2,19}

Considering the importance of PESCs, the study of their phase diagrams started long ago for a wide range of surfactants complexed by polymers or block copolymers. The complexity of this task is high due to multidimensionality, where effects of ionic strength, cosolvent, cosurfactants and charge could be taken into account.^{5,6,19,20,23–25} Even if the debate about whether PESCs are at equilibrium or not is still open,³ the study of their phase diagram has long been addressed using a classical thermodynamic approach, involving a systematic parametric study and equilibration times. However, more recent considerations question the importance of crossing phase boundaries under non-equilibrium conditions.^{3,4} This is motivated by both practical considerations on applications and fundamental questioning.³ If non-equilibrium transitions are a recent concern in PESCs³, they are in fact a major concern in the broader field of macromolecular complexation:^{26–28} molecular dynamics and diffusion-limited processes open again, under a new perspective, old questions such as possible shift of the

surfactant's phase boundary, promotion of a new surfactant's phase but also PESC disassembling or promotion of a new PESC phase.

The micelle-to-vesicle transition is particularly interesting because, while being classical in lyotropic surfactant and lipid phases,^{24,29} it could be exploited in delivery applications under non-equilibrium conditions. Interestingly, non-equilibrium micelle-to-vesicle transitions are well-known,³⁰ however, to the best of our knowledge, they were rarely investigated in P ESCs, even under pseudo-equilibrium conditions. The equilibrium phase diagram of ethoxy fatty acids in aqueous solutions displayed a pH-dependent micelle-to-vesicle transition,³¹ but the same transition was not observed in the presence of polyelectrolytes,³² thus confirming the yet unpredictable effect of polyelectrolytes on surfactants' phase diagram. This is particularly true in the case of lipid bilayer membranes, of which the physical properties, including the local composition, defects, segregation and bending energy depend on the polyion.^{24,33–36} Even if the complexity of the interactions between polyelectrolytes and (soft) interfaces has been addressed for decades,^{36–38} predicting the equilibrium curvature in P ESCs³ is still a challenge.^{39,40}

Fibrillation of low-molecular weight compounds is also another important field of research, from both applicative (hydrogelation)⁴¹ and fundamental (non-equilibrium phase transitions)⁴² perspectives. Development of P ESCs from low-molecular weight gelators is still a virgin field of research and questioning the interactions between polyelectrolytes and self-assembled fibers has only started with recent works.⁴³

In a series of recent communications, many authors have addressed the solution self-assembly of microbial glycolipid biosurfactants.^{44–46} These molecules have a multiple interest in the field of P ESCs: they are biobased and biodegradable amphiphiles⁴⁷ with a rich phase diagram and stimuli responsiveness. For these reasons they are highly prompt for the development of biocompatible P ESCs but also for the study of non-equilibrium phase transitions in complex systems, both aspects generating an increasing interest in the community.^{3,7} In particular, we have shown that acidic C18:1 sophorolipids, which form a stable micellar phase in a broad pH range,^{46,48,49} form pH-responsive complex coacervates in the presence of both synthetic and natural polyamines.⁵⁰ Interestingly, sophorolipid analogues have a richer, pH-stimulated, phase diagram including micelle-to-vesicle, micelle-to-fiber and micelle-lamellar transitions.^{46,49,51}

In this work, we explore the stability of a polyelectrolyte-surfactant complex coacervate at two distinct iso-compositional phase boundaries, micelle-vesicle and micelle-fiber, where phase transition is triggered by pH. To do so, we use two microbial glycolipid biosurfactants in

the presence of three cationic polyelectrolytes (PEC). Turbidimetric analysis, cryogenic transmission electron microscopy (cryo-TEM) and pH-resolved *in situ* small angle X-ray scattering (SAXS) using synchrotron radiation experiments show that complex coacervates are only stable in the micellar region of both glycolipids' phase diagram. However, if the lipid undergoes a micelle-to-vesicle transition, we observe a complex coacervate (*Co*) to multilamellar walls vesicles (*MLWV*) (*Co*-to-*MLWV*) phase transition. If the lipid undergoes a micelle-to-fiber transition, on the contrary, the coacervate disassembles and the glycolipid's fiber phase coexists with the polyelectrolyte, with no apparent interactions, against the literature's expectations.⁴³ Finally, this work demonstrates the use of biobased surfactants for the development of sustainable PESCs.

Experimental section

Chemicals

In this work we use glycolipids G-C18:1 ($M_w = 620 \text{ g mol}^{-1}$), made of a single β -D-glucose hydrophilic headgroup and a C18 fatty acid tail (monounsaturated in position 9,10), and SL-C18:0 ($M_w = 460 \text{ g mol}^{-1}$), composed of a sophorose headgroup and a stearic acid derivative. From alkaline to acidic pH, the former undergoes a micelle-to-vesicle phase transition⁴⁶ while the latter undergoes a micelle-to-fiber phase transition.⁵² The syntheses of sophorolipid SL-C18:0 and glucolipid G-C18:1 are respectively described in Ref ⁵² and ⁵¹, where the typical ^1H NMR spectra and HPLC chromatograms are also given. The compounds used in this work have a molecular purity of more than 95%.

The cationic polyelectrolytes (PEC) used in this work are chitosan, obtained from the deacetylation of chitin from crustaceans' shells, poly-L-lysine, widely used in biomedical field, and polyethylenimine. Chitosan oligosaccharide lactate (CHL) ($M_w \approx 5 \text{ KDa}$, $pK_a \sim 6.5$)⁵³ with a deacetylation degree >90%, (PLL) hydrobromide ($M_w \approx 1-5 \text{ KDa}$, $pK_a \sim 10-10.5$)⁵⁴ and polyethylenimine (PEI) hydrochloride (linear, $M_w \approx 4 \text{ KDa}$, $pK_a \sim 8$)⁵⁵ are purchased from Sigma-Aldrich. All other chemicals are of reagent grade and are used without further purification.

Preparation of stock solutions

SL-C18:0 ($C = 5 \text{ mg mL}^{-1}$), G-C18:1 ($C = 5 \text{ mg mL}^{-1}$, $C = 20 \text{ mg mL}^{-1}$), CHL ($C = 2 \text{ mg mL}^{-1}$), PLL ($C = 5 \text{ mg mL}^{-1}$, $C = 20 \text{ mg mL}^{-1}$), and PEI ($C = 5 \text{ mg mL}^{-1}$) stock solutions are prepared by dispersing the appropriate amount of each compound in the corresponding amount

of Milli-Q-grade water. The solutions are stirred at room temperature ($T = 23 \pm 2$ °C) and the final pH is increased to 11 by adding a few μL of NaOH ($C = 0.5$ M or $C = 1$ M).

Preparation of samples

Samples are prepared at room temperature ($T = 23 \pm 2$ °C) by mixing appropriate volume ratios of the lipid (SL-C18:0 or G-C18:1) stock solutions at pH 11 and cationic polyelectrolyte stock solutions (PEC), as defined in Table 1. The final total volume is generally set to $V = 1$ mL or $V = 2$ mL, the solution pH is about 11 and the final concentrations are given in Table 1. The pH of the mixed lipid-PEC solution is eventually decreased by the addition of 1-10 μL of a HCl solution at $C = 0.5$ M or $C = 1$ M. pH has been changed by hand and by mean of a push-syringe device. The rate at which pH is changed is generally not controlled although it is in the order of several $\mu\text{L}\cdot\text{min}^{-1}$. Differently than in other systems,^{31,56} we did not observe unexpected effects on the PESC structure to justify a tight control over the pH change rate.

Table 1 – Relative volumes of lipid and cationic polyelectrolyte (PEC) solutions to mix to obtain given concentrations

Volume			Concentration	
Lipid stock solution / mL	PEC stock solution / mL	Water / mL	$C_{\text{Lipid}} / \text{mg}\cdot\text{mL}^{-1}$	$C_{\text{PEC}} / \text{mg}\cdot\text{mL}^{-1}$
0.5	0.5	0	2.5 or 10	2.5 or 10
	0.25	0.25	2.5	1.25
	0.125	0.375	2.5	0.625

Turbidimetric titration using UV-Vis spectroscopy

The influence of pH and concentration of PEC on the formation of coacervate droplets is investigated by measuring the absorbance at a wavelength of $\lambda = 450$ nm. Data are recorded at room temperature ($T = 23 \pm 2$ °C) using a UV/Vis spectrophotometer (UVIKON XL, BioTek). Preparation of the samples for these experiments is the same as described above, however, the final concentration of the lipid is systematically set at $C = 2.5 \text{ mg}\cdot\text{mL}^{-1}$, while the final concentrations of the PEC range between $0.25 < C / \text{mg}\cdot\text{mL}^{-1} < 1$ for CHL and $0.63 < C / \text{mg}\cdot\text{mL}^{-1} < 2.5$ for PLL and PEI. The titrated volume is systematically $V = 1$ mL. The pH of each lipid-PEC mixed solution is decreased progressively by the manual addition of small amounts (V

<10 μL) of HCl = 0.1 M. The turbidity curves are recorded after each pH variation. Each solution is stirred before analysis, which is however performed at rest under static conditions, thus favoring sedimentation during the measurement. The turbidity curve of control lipid and PEC solutions is also measured as a function of pH.

Turbidimetric titration using Light Scattering (LS) and ζ -potential

To avoid sedimentation, we have repeated the turbidimetric titration experiment on selected samples using the automatic titration unit MPT-2 of a Malvern Zetasizer Nano ZS90 (Malvern Instruments Ltd, Worcestershire, UK) instrument, equipped with a 4 mW He-Ne laser at a wavelength of λ = 633 nm, measuring angle, θ = 90°, temperature, T = 25°C, and the signal is never attenuated throughout the entire experiment. The sample solution (V = 7 mL) is contained in an external beaker and pumped with a peristaltic pump through the ζ -potential cuvette cell located in the instrument for analysis. pH is adjusted in the beaker under by adding aliquots of V = 6 μL of a HCl solution at C = 0.5 M and controlled by the MPT-2 Zetasizer software. The beaker undergoes gentle stirring to avoid the formation of air bubbles in the flow-through tubing system and, consequently, in the ζ -potential cuvette. Avoiding air bubbles in the cuvette is crucial and accurately inspected throughout the experiment. Light scattering and ζ -potential are simultaneously recorded between each pH variation while the sample solution is continuously pumped through the cuvette. The latter action guarantees that sedimentation does not occur neither in the cuvette nor in the external beaker.

pH-resolved *in situ* Small angle X-ray scattering (SAXS)

In situ SAXS experiments during pH variation are performed at room temperature on two different beamlines. The B21 beamline at Diamond Light Source Synchrotron (Harwell, England) is employed using an energy of E = 13.1 keV and a fixed sample-to-detector (Eiger X 4M) distance of 2.69 m. The Swing beamline at Soleil Synchrotron (Saint-Aubin, France) is employed using an energy of E = 12 keV and a fixed sample-to-detector (Eiger X 4M) distance of 1.995 m. For all experiments: the q -range is calibrated to be contained between $\sim 5 \cdot 10^{-3} < q/\text{\AA}^{-1} < \sim 4.5 \cdot 10^{-1}$; raw data collected on the 2D detector are integrated azimuthally using the in-house software provided at the beamline and so to obtain the typical scattered intensity $I(q)$ profile, with q being the wavevector ($q = 4\pi \sin \theta / \lambda$, where 2θ is the scattering angle and λ is the wavelength). Defectuous pixels and beam stop shadow are systematically masked before azimuthal integration. Absolute intensity units are determined by measuring the scattering

signal of water ($I_{q=0} = 0.0163 \text{ cm}^{-1}$). SAXS profiles are manipulated with SasView software, version 3.1.2, available at the developer's website (sasview.org).

The same sample experimental setup is employed on both beamlines: the sample solution ($V = 1 \text{ mL}$) with the lipid and PEC at their final concentration and pH ~ 11 is contained in an external beaker under stirring at room temperature ($T = 23 \pm 2^\circ\text{C}$). The solution is continuously flushed through a 1 mm glass capillary using an external peristaltic pump. The pH of the solution in the beaker is changed using an interfaced push syringe, injecting microliter amounts of a 0.5 M HCl solution. pH is measured using a micro electrode (Mettler-Toledo) and the value of pH is monitored live and manually recorded from the control room via a network camera pointing at the pH-meter located next to the beaker in the experimental hutch. Considering the fast pH change kinetics, the error on the pH value is ± 0.5 .

Polarized Light Microscopy (PLM)

PLM experiments are performed with a transmission Zeiss AxioImager A2 POL optical microscope. A drop of the given sample solution is deposited on a slide covered with a cover slip. The microscope is equipped with a polarized light source, crossed polarizers and an AxioCam CCD camera.

Cryogenic transmission electron microscopy (cryo-TEM)

Cryo-TEM experiments are carried out on an FEI Tecnai 120 twin microscope operated at 120 kV and equipped with a Gatan Orius CCD numeric camera. The sample holder is a Gatan Cryoholder (Gatan 626DH, Gatan). Digital Micrograph software is used for image acquisition. Cryofixation is done using a homemade cryofixation device. The solutions are deposited on a glow-discharged holey carbon coated TEM copper grid (Quantifoil R2/2, Germany). Excess solution is removed and the grid is immediately plunged into liquid ethane at -180°C before transferring them into liquid nitrogen. All grids are kept at liquid nitrogen temperature throughout all experimentation. Cryo-TEM images have been treated and analyzed using Fiji software, available free of charge at the developer's website.⁵⁷

Results

Deacetylated acidic sophorolipid SL-C18:0 (saturated) and glucolipid G-C18:1 (monounsaturated) are two microbial glycolipid biosurfactants used in this work and both containing a free carboxylic acid chemical function (Figure 1). Alkaline solutions of SL-C18:0 and G-C18:1 at room temperature and concentrations below 10 wt% are characterized by a major micellar phase. At $\text{pH} < 7.4$, SL-C18:0 self-assembles into crystalline twisted ribbons, while at $\text{pH} < 6.2$ G-C18:1 self-assembles into vesicles.^{46,51,52}

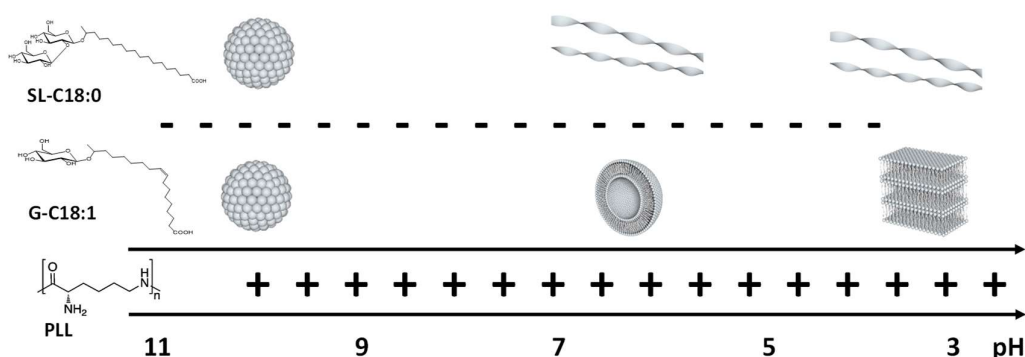


Figure 1 – pH-dependent phase and (negative) charge diagram for SL-C18:0 and G-C18:1 microbial glycolipids biosurfactants at $C < 10$ wt% and room temperature. The (positive) charge of PLL polyelectrolyte is also indicated as a function of pH

Figure 1 summarizes the pH-dependent phase and charge diagram of SL-C18:0 and G-C18:1 glycolipids, which are negatively charged above $\text{pH} \sim 4.5$, due to their carboxylate function. PLL polyelectrolyte is on the contrary positively charged below $\text{pH} 10$, water-soluble and it adopts a random coil conformation. The other PEC employed in this work, CHL and PEI, have a similar behavior, except for their pK_a values, which are respectively 6.5 and 8. The charge complementarity between the glycolipids and PEC in a given pH range leads to an expected electrostatic interaction, which was shown to form glycolipid-PEC complex coacervates, when acidic deacetylated monounsaturated sophorolipids (SL-C18:1) were employed.⁵⁰ To explore whether SL-C18:0 and G-C18:1 glycolipids form complex coacervates, and whether their pH-induced phase transition has a potential impact on the coacervate structure, we perform a series of pH-stimulated experiments on mixtures of each glycolipid and PEC. The main body of this work summarizes the results obtained with PLL, while the data collected on CHL and PEI are only briefly discussed and presented as supporting information, as they support the main conclusions obtained with PLL.

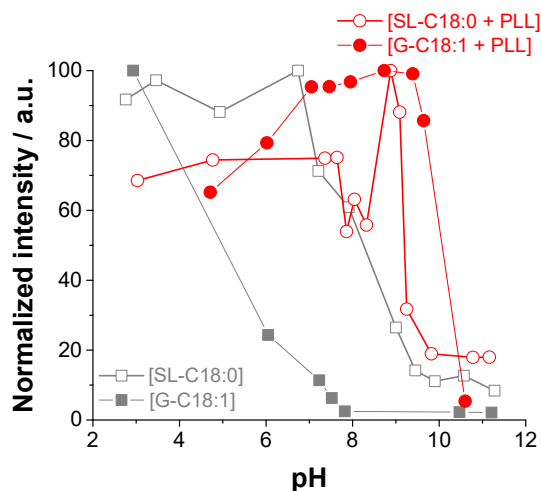


Figure 2 – Room temperature turbidimetric analysis performed by UV-Vis spectroscopy of SL-C18:0 and G-C18:1 glycolipid solutions with and without PLL as a function of pH. The typical sample preparation is described in the materials and method section. The final lipid and PEC concentrations are $C_{G-C18:1} = C_{SL-C18:0} = 2.5 \text{ mg}\cdot\text{mL}^{-1}$, $C_{PLL} = 1.25 \text{ mg}\cdot\text{mL}^{-1}$. pH is decreased from 11 to 3.

Figure 2 presents the pH-resolved turbidimetric analysis on control lipid ([SL-C18:0] and [G-C18:1]) solutions (grey symbols) and mixtures of lipids with PLL (red symbols). As a general result, control solutions display poor scattering (micellar phase) above pH ~ 8 and ~ 9 for, respectively, G-C18:1 and SL-C18:0; on the contrary, scattering is maximized below pH ~ 6 and ~ 7 for, respectively, G-C18:1 and SL-C18:0. These results are coherent with their known micelle-to-vesicle⁴⁶ and micelle-to-fiber⁵² phase transitions. We must notice that scattering of SL-C18:0 fibers below pH 7 is weaker than what it should be⁵² and this is due to sedimentation issues during the experiment. A specific comment on this aspect is associated to Figure S 1 in the Supporting Information and where pH-resolved experiments are performed *in situ* in the light scattering apparatus. Finally, scattering of PLL alone is negligible on the entire pH range and for this reason it is not displayed in Figure 2. Mixtures of SL-C18:0, or G-C18:1, and PLL highlight a region of strong scattering (red symbols) already at $9 < \text{pH} < 10$, that is at least two to three orders of pH higher than the controls, and indicating that both glycolipids preferentially interact with PLL under these pH conditions, according to the likely hypothesis of charge matching schematized in Figure 1. The data in Figure 2, reported for final concentrations of lipid and PLL of, respectively, $2.5 \text{ mg}\cdot\text{mL}^{-1}$ and $1.25 \text{ mg}\cdot\text{mL}^{-1}$, are quite robust and reproducible for a broader range of lipid-to-PLL mass ratios, as shown in Figure S 2. Similar results were also reported for SL-C18:1 sophorolipids and PEC solutions⁵⁰ and for a broad range of micelle-polyelectrolyte complex coacervates.²¹ pH-resolved *in situ* ζ -potential measurements are

employed to show mutual interactions by charge-matching (Figure S 3). The lipid control solutions display the presence of negatively-charged colloids between pH 10 and 4, while lipid and PLL mixed solutions show an overall charge neutralization process occurring since pH 10, indirectly demonstrating the interaction between the lipid and polyelectrolyte.

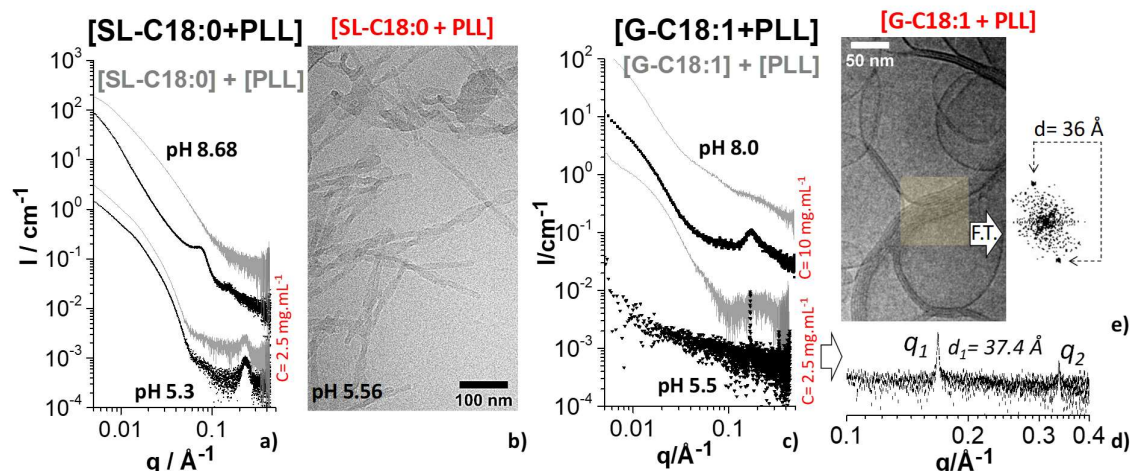


Figure 3 –a) Black curves: SAXS profiles recorded for a co-assembled mixture of [SL-C18:0 + PLL] at pH above and below 7. Grey curves: arithmetical summation of the SAXS profiles each recorded individually on the control solutions of [SL-C18:0] and [PLL] at pH below and above 7. An artificial offset has been added for sake of clarity. b) Cryo-TEM image of the co-assembled [SL-C18:0 + PLL] solution at pH 5.56. Concentrations are $C_{\text{SL-C18:0}} = C_{\text{PLL}} = 2.5 \text{ mg mL}^{-1}$ at both pH values. c) Black curves: SAXS profiles recorded for a co-assembled mixture of [G-C18:1 + PLL] (black curves) at pH above and below 7. Grey curves: arithmetical summation of the SAXS profiles each recorded individually on the control solutions of [G-C18:1] and [PLL] at pH below and above 7. An artificial offset has been added for sake of clarity. d) Highlighted high- q region of [G-C18:1 + PLL] at pH= 5.5. e) Cryo-TEM image of the co-assembled [G-C18:1 + PLL] solution at pH 4.70. Concentrations are $C_{\text{G-C18:1}} = C_{\text{PLL}} = 2.5 \text{ mg mL}^{-1}$ at pH= 5.50 and $C_{\text{G-C18:1}} = C_{\text{PLL}} = 10 \text{ mg mL}^{-1}$ at pH= 8.0. Image has been analyzed using Fiji software.⁵⁷

A combination of SAXS and cryo-TEM experiments (Figure 3) is used to study the structure of SL-C18:0 and G-C18:1 with PLL in the regions of strong light scattering and below pH 7 (Figure 2). The SAXS profiles (Figure 3a and c) show the signals recorded at acidic and basic pH, where black curves labelled [SL-C18:0 + PLL] and [G-C18:1 + PLL] correspond to co-assembled lipid:PLL PESCs solutions. Grey curves labelled [SL-C18:0] + [PLL] and [G-C18:1] + [PLL] correspond to the arithmetic sum of the SAXS profiles recorded on the individual lipid and PLL controls solutions separately. Figure S 4 illustrates the SAXS profiles of the individual SL-C18:0 (blue symbols) and PLL (red symbols) control solutions recorded at pH 5.50 and 8.68 as well as their arithmetic sum (grey symbols). The difference in concentration between the G-C18:1 system at pH > 7 ($C = 10 \text{ mg mL}^{-1}$) and the rest ($C = 2.5$

mg·mL⁻¹, Figure 3a,c) is simply a matter of signal-to-noise ratio. The corresponding SAXS profile collected at $C_{\text{G-C18:1}} = C_{\text{PLL}} = 2.5 \text{ mg·mL}^{-1}$ and pH 8.0 is given in Figure S 5 and it indeed shows a similar profile but with a poorer signal-to-noise, probably due to a combination of poor contrast and low concentration.

In the micellar region of the phase diagram (pH > 8), both glycolipids in their mixture with PLL have SAXS profiles characterized by a strong low- q scattering and a broad peak (black curves in Figure 3a,c). The peak is centered at $q = 0.078 \text{ \AA}^{-1}$ ($d = 80.5 \text{ \AA}$) while a second peak can be observed at $q = 0.15 \text{ \AA}^{-1}$ ($d = 41.8 \text{ \AA}$) for SL-C18:0 and at $q = 0.174 \text{ \AA}^{-1}$ ($d = 36.1 \text{ \AA}$) for G-C18:1. Comparison between the co-assembled lipid and PLL solution (black curves) with the corresponding controls (grey curves in Figure 3a,c above pH 8) at basic pH shows that, if low- q scattering is generally comparable, the correlation peak is unique only in the co-assembled solutions and never observed for the pure glycolipids. The presence of a correlation peak is actually general and not only observed with PLL. For instance, SL-C18:0 (at basic pH) systematically shows two broad correlation peaks centered at $q = 0.078 \pm 0.002 \text{ \AA}^{-1}$ and at $q = 0.15 \pm 0.10 \text{ \AA}^{-1}$ when it is co-assembled with PLL, PEI or CHL (Figure S 6a). These peaks, common in scattering experiments of micelle-polyelectrolyte complex coacervates,²¹ are generally associated to the structure of the co-assembled lipid with PEC. To better understand the origin of the peak at basic pH in the SAXS experiments, we study the structure of [SL-C18:0 + PLL] and [G-C18:1 + PLL] using cryo-TEM.

The typical cryo-TEM images of [SL-C18:0 + PLL] and [G-C18:1 + PLL] at basic pH are shown in Figure 4, while additional images are given in Figure S 7. All samples, irrespective of the pH value, are characterized of large spherical colloidal (sc) structures, of diameter larger than 1000 \AA , embedded in a medium, which often displays a fingerprint-like texture (Figure 4 and Figure S 7a,d,e). Regions of much smoother, untextured, background are however observed, as well (Figure S 7b,c). sc display as dense, untextured, more contrasted, objects. One can occasionally observe, mainly in [SL-C18:0 + PLL] systems, a third type of component, constituted of agglomerated, highly contrasted, particles of typical primary size contained between 20 nm and 50 nm (Figure 4 and Figure S 7b). Both aggregated particles and sc of similar texture, size, morphology and contrast were largely documented using cryo-TEM by others^{22,58,59} and by us⁵⁰ in polyelectrolyte-surfactant complex coacervates.

The entire set of cryo-TEM images that we have recorded on glycolipids SL-C18:0 and G-C18:1 co-assembled with PLL or PEI at basic pH show the same type of structures as presented in Figure 4 and Figure S 7. From a macroscopic point of view, all samples form a stable suspension of liquid spherical droplets similarly to our previous results,⁵⁰ rather than a

solid precipitate. The combination of these pieces of evidence³ indicate that complex coacervation systematically occurs in the micellar region of the glycolipids phase diagram. Concerning CHL, we cannot draw a clear-cut conclusion due to the fact that this compound precipitates above pH 7⁶⁰ and its interactions with glycolipids in the alkaline region are at the moment unclear. The SAXS data corresponding to [SL-C18:0 + CHL] shown in Figure S 6 confirm this assumption: the typical correlation peaks, clearly observed in the PLL and PEI systems, can be hardly identified. However, complementary data recorded on the [G-C18:1 + CHL] system, and presented elsewhere,⁶¹ still suggest the formation of complex coacervate, probably

We are at the moment unable to draw a general conclusion in terms of which pH, or type of glycolipid, has a preferential impact on the formation of *sc* compared to dense aggregated structures. Dense aggregates are generally attributed to dehydrated complex coacervates^{22,50} formed on the coacervation plateau, while *sc* structures are attributed to hydrated complex coacervates, probably during formation, in their liquid phase.⁵⁹ In the present work, for the [SL-C18:0 + PLL] system, for instance, we do not identify such a similar logic as we observe dense coacervates and *sc* irrespectively of the pH value (Figure S 7a-c), or even coexisting at the same pH (Figure 4). This aspect may be explained by the small coacervation plateau (Figure 2, Figure S 1 and Figure S 2) and by the likely difficulty of reaching a homogeneous, single-phase, medium in the present pH-driven experiments carried out of equilibrium. Nonetheless, dense structures are always superimposed to a clear background, as described by Dubin *et al.*,²² while the fingerprint-like background is systematically associated to *sc* structures, independently of the glycolipid employed. This is nicely shown for [SL-C18:0 + PLL] in Figure 4, where a clear-cut frontier delimitates dense coacervates on top from *sc* on the bottom, the former being embedded in a smooth background while the latter embedded in a fingerprint-like background. In line with Dubin *et al.*,⁵⁹ we speculate that the composition of the fingerprint-like background is rich in glycolipid, while the *sc* are rather rich in PEC. To better understand the structure of the fingerprint-like background and the *sc* and dense aggregates, we propose hereafter a crossed SAXS-cryo-TEM analysis of both [SL-C18:0 + PLL] and [G-C18:1 + PLL] systems.

The Fourier Transform (F.T.) of the fingerprint-like region in the [SL-C18:0 + PLL] system (panel 2 in Figure 4a) provides a broad ring corresponding to *d*-spacing between 80 Å and 40 Å, while the dense coacervate region, panel 1 in Figure 4a, provides an additional ring of *d*-spacing between 30 Å and 40 Å. Comparison between the *d*-spacing values estimated from cryo-TEM with *d*-spacing obtained by SAXS (*d*= 80.5 Å and *d*= 41.8 Å, Figure 3a) confirms

the hypothesis according to which the correlation peak in SAXS is reasonably associated to the structure of complex coacervates. Interestingly, the q -values are in a 1:2 ratio, generally found in lamellar stacking but excluded in this system by cryo-TEM arguments. Correlation peaks with q -values in 1:2 ratio were observed before in β -lactoglobulin(β LgA)-pectin complex coacervates⁶² and were attributed to the presence of β LgA clusters coexisting with ordered protein-to-protein correlations observed inside the clusters. In the present case, the d -spacing at $d = 41.8 \text{ \AA}$ can be reasonably attributed to the dense aggregates (panel 1 in Figure 4a), most likely composed of tightly packed SL-C18:0 micelles embedded in the polyelectrolyte matrix adopting a globular conformation (Figure 4a).²² This hypothesis is also in agreement with the typical cross-sectional diameter of SL-C18:0 micelles ($\sim 35 \text{ \AA}$)⁴⁶ and with the previously-proposed colloid cluster model in complex coacervates.²¹ The colloid cluster model is unfortunately not able to explain neither larger d -spacing values nor the fingerprint-like textured background. The only way to explain a d -spacing value corresponding to approximately twice the size of a SL-C18:0 molecule is by considering a “pearl-necklace”-like structure, proposed long time ago for polyelectrolyte-micelles complexes,^{4,7,32,63} and adapted to the present (Figure 4a) to adapt the larger experimental d -spacing.

The Fourier Transform (F.T.) of the fingerprint-like region, panel 3 in Figure 4b, in the [G-C18:1 + PLL] system, also shows a broad ring with d -spacing values contained between 40 \AA and 60 \AA , a range which is overestimated by at least a factor 1.5 with respect to the d -spacing value measured by SAXS ($d = 36.1 \text{ \AA}$). Despite such a discrepancy, the lack of other organized structures in cryo-TEM and the lack of other correlation peaks in SAXS suggest that the existing correlation peak should be attributed to the textured background identified in panel 3 in Figure 4b. However, a spontaneous question arises: why is the d -spacing value associated to the textured region in the [G-C18:1 + PLL] system correlated to the size of a single G-C18:1 molecule^{46,51} and not to twice its size, as found for [SL-C18:0 + PLL]? The only reasonable answer that we can propose is the possibly different packing of G-C18:1 around the polyelectrolyte: instead of the expected micellar packing, G-C18:1 could form interdigitated wormlike micelles stabilized by the polyelectrolyte (scheme in Figure 4b), as also discussed for other polyelectrolyte-micelle complexes.^{3,4,20,64} This hypothesis is not outrageous because wormlike micelles are experimentally found as a transitory phase during the micelle-to-vesicle transition in the PEC-free G-C18:1 aqueous system.⁴⁶ Analysis of the slope in, or even modelling of, SAXS profiles could certainly help to corroborate the hypotheses of “pearl-necklace” (Figure 4a) and wormlike (Figure 4b) models, as proposed by other authors.^{32,65} Any tentative analysis of our SAXS data in the log-log scale provide a dependence of the intensity

on q around -3, which is typically found for fractal structures but which, unfortunately, does not bring any meaningful information on the present system. Cryo-TEM experiments show a multiphasic medium with coexistence of more than one structural intermediate, thus making a clear-cut interpretation of the SAXS profile very hard, if not impossible.

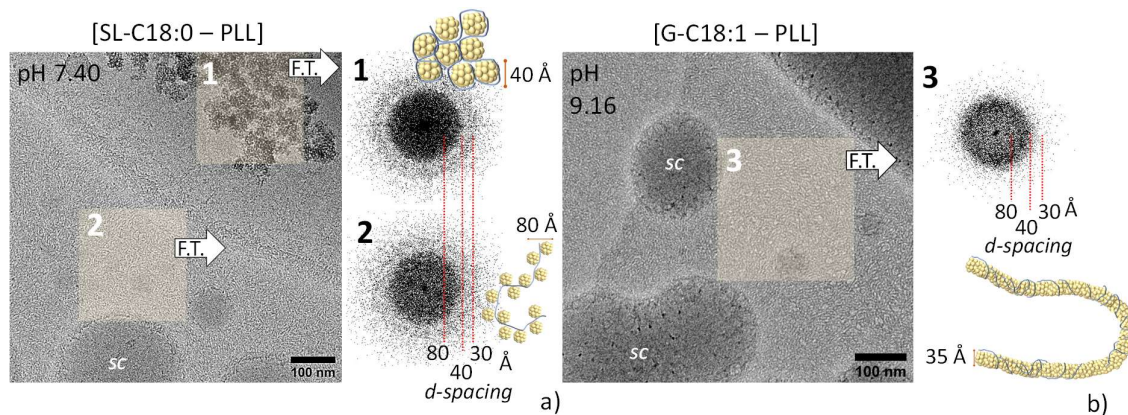


Figure 4 – Typical cryo-TEM images recorded at a) pH 7.40 for [SL-C18:0 + PLL] and at b) pH 9.16 for [G-C18:1 + PLL] co-assembled solutions. Concentrations are $C_{\text{SL-C18:0}} = C_{\text{G-C18:1}} = 2.5 \text{ mg mL}^{-1}$ and $C_{\text{PLL}} = 1.25 \text{ mg mL}^{-1}$. Panels 1 through 3 identify regions where Fourier Transform (F.T.) is performed. F.T. images are indicated by the arrows on the right-hand side of each cryo-TEM image.

Experiments performed at acidic pH are shown in Figure 3a,b (SAXS: black curve, pH 5.30; cryo-TEM: pH 5.56) for the [SL-C18:0 + PLL] mixture and in Figure 3c-e (SAXS: black curve, pH 5.50; cryo-TEM: pH 4.70) for the [G-C18:1 + PLL] mixture. In the SL-C18:0 system, SAXS shows a strong low- q scattering and a diffraction peak at $q = 0.24 \text{ Å}^{-1}$. The same exact profile is observed for the [SL-C18:0] + [PLL] control signal (grey curve, pH 5.30, Figure 3a) and reported for a typical aqueous solution of SL-C18:0 twisted ribbons, the peak being attributed to the repeating inter-lipid layer distance within each ribbon.⁵² Twisted ribbons of similar size (cross section $\sim 150 \text{ Å}$) and morphology compared to the previous findings of pure SL-C18:0 system at acidic pH are actually observed in the corresponding cryo-TEM images (Figure 3c). Knowing that SL-C18:0 assembles into a fibrillary state at acidic pH, one can reasonably suppose that SL-C18:0 does not interact with PLL under these conditions and the micelle-to-fiber self-assembly process (Figure 1) occurs independently whether SL-C18:0 is in a free micellar^{46,52} or in PESCs complex coacervates. At the moment, we have no evidence, neither by SAXS nor by cryo-TEM, that SL-C18:0 fibers interact in any way with PEC, differently than what was reported for bile salts fibers complexed with block copolymers.⁴³ We could explain this evidence by the fact that self-assembled fibers are only composed of the COOH form of SL-C18:0 and they are thus neutral objects, which do not interact with PEC.

This statement seems to be in contrast with ζ -potential experiments performed on the SL-C18:0 system below pH 7 (Figure S 3) and showing an overall negative charge. However, one should be aware that ζ -potential experiments are not structure-selective and we have no direct proof that the global negative charge is specifically associated to fibrillary structures rather than to an average medium composed of fibers, micellar and free SL-C18:0 molecules.

The SAXS profile of the [G-C18:1 + PLL] at pH 5.50 (black curve, Figure 3c,d) is on the contrary very different than the corresponding [G-C18:1] + [PLL] control signal (grey curve, pH 5.50, Figure 3c): the mixture displays two sharp peaks at $q_1 = 0.17 \text{ \AA}^{-1}$ and $q_2 = 0.34 \text{ \AA}^{-1}$ (Figure 3d), referring to the (100) and (200) reflection of a lamellar order, while the control signal has the typical profile of single-wall vesicles, expected for G-C18:1 in water at concentration below 10 wt% and $\text{pH} < 7$.^{46,51} The $q_1:q_2 = 0.5$ and the sharpness of the peaks ($\Delta q = 1.4 \cdot 10^{-3} \text{ \AA}^{-1}$) strongly suggest the presence of extended lamellar domains, never observed for this compound alone prepared under the same conditions. The corresponding cryo-TEM image in Figure 3e interestingly shows the systematic massive presence of vesicular objects having a thick lamellar wall (white arrows in Figure 3e), as similarly found in lipoplexe systems,^{2,19} and other multilamellar walls vesicle PESCs.⁴ Cryo-TEM excludes the presence of a flat lamellar phase, or condensed platelets. A more detailed study of the [G-C18:1 + PLL] material under acidic pH conditions are reported elsewhere.⁶¹

pH-resolved in situ study of the phase transition

SAXS experiments coupled to cryo-TEM imaging performed at basic and acidic pH (Figure 3) provide some structural features, but they do not inform on the possible structural and morphological transitions of the colloidal structures during pH variation. To do so, we perform a pH-resolved *in situ* analysis (detailed use of the setup is given in the materials and method section) of the PESCs from alkaline to acidic pH. The corresponding SAXS 2D contour plots are presented in Figure 5.

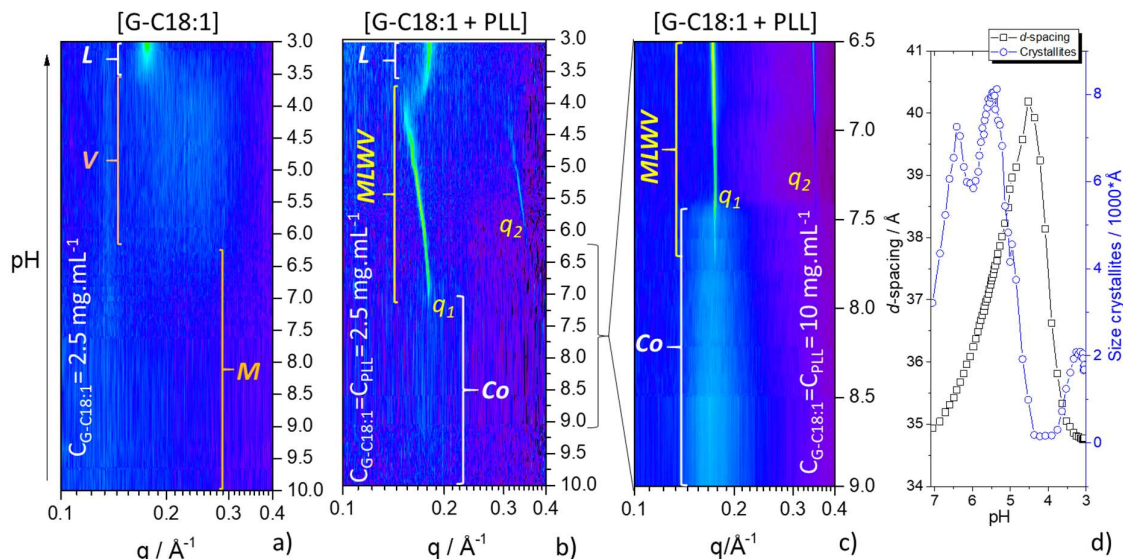


Figure 5 – pH-resolved (pH is changed from alkaline to acidic) *in situ* SAXS 2D contour plots of a) G-C18:1 control solution ($C = 2.5 \text{ mg mL}^{-1}$), b) [G-C18:1 + PLL] sample at $C_{\text{G-C18:1}} = C_{\text{PLL}} = 2.5 \text{ mg mL}^{-1}$ and c) [G-C18:1 + PLL] sample at $C_{\text{G-C18:1}} = C_{\text{PLL}} = 10 \text{ mg mL}^{-1}$. *M*: Micellar phase; *V*: Vesicles phase; *L*: Lamellar phase; *MLWV*: Multilamellar wall vesicle phase; *Co*: Complex coacervate phase. d) Evolution of d -spacing and size of crystallites at $\text{pH} < 7$ for experiment in b). d -spacing is obtained from $6.28/q_1$ while size of crystallites is obtained using the Scherrer formula $(0.9 \cdot 6.28)/FWHM$, where $FWHM$ is the full width at half maximum of peak q_1 given in \AA^{-1} units. q_1 and $FWHM$ have been obtained by mean of a Lorentzian peak fitting procedure.

The contour plot ($0.1 < q / \text{\AA}^{-1} < 0.4$) concerning the pH dependency of G-C18:1 control sample solution is shown in Figure 5a. The pH region between pH 10 and ~ 6.5 is characterized by no distinct signal in the contour plot representation, as expected, because G-C18:1 forms a micellar, *M*, phase in this pH range.^{46,51} Below pH ~ 6.5 and until pH ~ 3.5 , the contour plot shows a broad signal, characterizing the vesicle, *V*, phase and corresponding to the oscillation of the vesicle membrane form factor (grey profile, pH 5.5, Figure 3c) and largely documented in Ref. ^{46,51}. Below pH ~ 3.5 , two sharp diffraction peaks at $q = 0.176 \text{ \AA}^{-1}$ and $q = 0.352 \text{ \AA}^{-1}$ (Figure S 8) refer to the (100) and (200) reflections of a lamellar order and characterize a lamellar phase, *L*, precipitate in solution.⁴⁶ In summary, the control G-C18:1 solution displays a micelle-to-vesicle-to-lamellar phase transition in agreement with our previous results.⁴⁶

The contour plot for the [G-C18:1 + PLL] PESC at $C = 2.5 \text{ mg mL}^{-1}$ is shown in Figure 5b. From pH 10 to about pH 7.5, the plot shows the dim signal of the broad ($\Delta q = 0.06 \text{ \AA}^{-1}$) correlation peak at $q = 0.171 \text{ \AA}^{-1}$ attributed to the *Co* phase. Figure S 5 better highlights the peak,

which is hardly observable in the contour plot due to a simple matter of plotting levels. The signal of the same phase is more intense and better identified at higher lipid and PLL concentration, as highlighted by the *Co* region between pH 9 and 7.5 in Figure 5c and Figure S 5. Below pH ~ 7.5 , two sharp diffraction peaks of full width at half maximum $\Delta q = 0.0015 \text{ \AA}^{-1}$, respectively corresponding to the first and second order reflections, q_1 and q_2 , of the multilamellar walls vesicle, *MLWV*, phase in Figure 3d,e, are observed until pH 4. Figure 5b shows that the position of q_1 (and q_2) varies continuously from $q_1 = 0.178 \text{ \AA}^{-1}$ at pH 7.5 to $q_1 = 0.157 \text{ \AA}^{-1}$ at pH 4, corresponding to a variation in d -spacing of 5 Å, between 35 Å to 40 Å (black squares in Figure 5d). Below pH 4, the contour plot is characterized by an abrupt jump in the q -value from 0.157 \AA^{-1} back to 0.176 \AA^{-1} , immediately stabilizing itself at 0.181 \AA^{-1} , and corresponding to a similar decrease in d -spacing of 5 Å, from 40 Å back to 35 Å.

The q_1 peak below pH 4 has the same features (position, invariance of the position towards pH, appearance in the same pH range) as the peak characterizing the *L* phase of the control G-C18:1 solution (Figure 5a). We then reasonably attribute it to the precipitation of the lipid *L* phase, probably without PLL, which is most likely expelled in the surrounding solution. This assumption will be discussed in more detail in the next paragraphs. All in all, the G-C18:1 lipid undergoes a pH-driven *Co*-to-*MLWV*-to-*L* phase transition when mixed with PLL. In fact, this result is more general and not restricted to PLL only: we find similar results for all other PEC tested in this study and discussed elsewhere.⁶¹

In comparison to G-C18:1, SL-C18:0-based PESCs behave in a completely different manner, because they are characterized by a straight micelle-to-fiber phase transition around pH 7. No structural or morphological continuity in the micelle-to-fiber phase transition is ever observed for this system, where micelles are more thought to play a reservoir role rather than a nucleation site.^{46,56} Interestingly, when SL-C18:0 is mixed with PLL, we also observe a systematic direct coacervate-to-fiber phase transition (Figure S 9), where the coacervate signal at basic pH fades away until the appearance of the typical fiber structural peak at $q = 0.229 \text{ \AA}^{-1}$ below pH 7.⁴⁶ This behavior follows the direct micelle-to-fiber phase transition observed for the SL-C18:0 control and we could reproduce it with all PEC employed in this work when they are mixed with this lipid.

Complex coacervate-to-Multilamellar wall vesicles (Co-to-MLWV) phase transition

The pH-resolved *in situ* SAXS experiments show a remarkably different behaviour of the G-C18:1 lipid in the presence of PLL with respect to the control. The latter undergoes a micelle-to-vesicle phase transition, driven by the carboxylate-to-carboxylic acid reaction upon

lowering the pH and inducing a conformational change of the lipid. Low curvature membrane (Figure 6b) morphologies are then favoured over high curvature micelles (Figure 6a), due to the progressive disappearance of repulsive electrostatic interactions, which indirectly impact the packing parameter of the lipid.^{18,66} Our data show that the same phenomenon occurs in the presence of PLL, when the lipid micelles are engaged in the formation of complex coacervates (Figure 6c). Upon lowering the pH, micelle-to-vesicle phase transition always occurs despite the presence of PLL; however, instead of forming single-wall vesicles, classically found in the control,⁵¹ we observe a *Co*-to-*MLWV* phase transition (Figure 6d).

The continuity in the phase transition and the isostructural and isodimensional correlations between the coacervate and *MLWV* phases is explicit in the 2D SAXS experiment at $C_{\text{G-C18:1}} = 10 \text{ mg mL}^{-1}$ (Figure 5c): the broad correlation peak of the *Co* phase at $q = 0.171 \text{ \AA}^{-1}$ fades away between pH 7.7 and 7.5 and it overlaps to the sharp diffraction peak of the *MLWV* phase at $q = 0.179 \text{ \AA}^{-1}$. Their position only shifts in $|q - q_1| = 0.007 \text{ \AA}^{-1}$ (1.6 Å) strongly suggesting an internal, progressive, restructuring of the coacervate into the *MLWV* (Figure 6c,d). The average *d*-spacing associated to the *q* range contained between 0.171 \AA^{-1} and 0.179 \AA^{-1} is $d = 35.9 \text{ \AA}$, in agreement with both the typical diameter of a G-C18:1 micelle and the thickness of its corresponding membrane,⁴⁶ but also to the length of a single lipid molecule, estimated to be 31.8 \AA using the Tanford relationship.^{51,67} G-C18:1 is a bolaform amphiphile and we have previously shown that its micellar structure is not a classical core-shell spheroid, where the diameter roughly corresponds to twice the size of the molecule,⁶⁸ but rather to a core-shell ellipsoid, where the diameter matches the size of each single lipid, a typical behavior in bolaamphiphiles (Figure 6a,c).^{46,68,69} In the meanwhile, we have also shown that, differently than bilayer-forming lipids, G-C18:1 forms vesicles with an interdigitated lipid layer (IL), of which the thickness corresponds to the size of a single molecule (Figure 6b,d).^{46,51,68,69} In light of these observations, the most reasonable hypothesis explaining the *Co*-to-*MLWV* transition is a local decrease in curvature due to the micelle-to-IL transition (Figure 6c,d) of G-C18:1. The driving force is the screening of electrostatic repulsions between adjacent carboxylate groups due to progressive acidification (Figure 6a,b). The residual negative charges in the membrane guarantee a charge density high enough to promote electrostatic attraction with the positively-charged PLL, as theoretically predicted and experimentally observed in polyelectrolyte systems at charged interfaces.^{38,70,71}

The equilibrium curvature in lipid-polyelectrolyte complexes depends on a subtle force balance between the bending modulus and electrostatic energy, which can be comparable.^{35,36,72} Polymers can have a significant impact on the bending energy of lipid bilayers in the case of

strong adsorption and large polymer volume fractions.³³ For charged systems in particular, the interplay between the bending stiffness of the lipid bilayer and the charge density of both the lipid bilayer and polyelectrolyte govern the overall free energy of the complex.^{4,24,35,36,72} As a consequence, it is not obvious to predict the equilibrium curvature in a complex polyelectrolyte-bilayer system at equilibrium,^{39,40} and this task becomes even harder, if not impossible, in non-equilibrium systems with variable surface charge density.

Micelles have a high charge density and a higher spontaneous curvature compared to vesicles. When the decrease in pH reduces the charge density inducing the micelle-to-vesicle phase transition, the PESC undergoes the *Co*-to-*MLWV* phase transition, meaning a decrease in spontaneous curvature. Interestingly, the pH region where this phenomenon occurs is the same in the control and in the complex, thus meaning that the contribution of the membrane bending energy prevails over the electrostatic energy contribution.³⁵ It is also interesting to note that [G-C18:1 + PLL] PESCs form vesicular (*MLWV*), and not flat, multilamellar objects. This is also not an obvious result and it can also be explained by the subtle interplay between the electrostatic and bending energies.^{34,36} The former is not large enough to counterbalance the membrane spontaneous tendency to bend; on the contrary, the magnitude of the latter, being proportional to the membrane bending rigidity,⁷³ is not high enough to drive the complex towards an infinitely small curvature, characterizing a flat structure.

In the description proposed by Brooks *et al.*³³, the effective bending energy can significantly vary in the case of strong adsorption and large volume fraction of the polymer, meaning that, in principle, the polymer could flatten the membrane. Other authors point at the importance of the charge ratio, Z , between the polyelectrolyte and the lipid but also at the persistence length, that is the rigidity, of the polymer:⁷ for small Z and flexible polymers, supramicellar aggregates like complex coacervates are favoured, while for high Z and rigid polymers, micellar rods or flat bilayers might be favoured. In the present work we observe the same phase *Co*-to-*MLWV* transition, whichever the polymer employed, may it be PLL or chitosan, the latter being considered as rigid.⁷ The ionic strength is not controlled but the pH change process generates salt concentrations generally below 100 mM, which are generally enough to keep the rigidity properties of the polyelectrolyte.⁷ The actual value of Z for our systems is harder to determine. A mere calculation based on the lipid and PEC concentrations and respective molecular weight indicates $Z < 1$, which is compatible, according to ref. ⁷, with the existence of complex coacervates. However, in these systems Z increases during pH variation because of the carboxylate-to-carboxylic reaction and in fact we are not able to quantify Z at a given pH simply because we cannot measure the actual surface charge density

and distribution in PESCs. On the basis of these considerations, we conclude that the impact of polymer adsorption (including strength, quantity, rigidity and screening) is not strong enough to prevent the micelle-to-vesicle transition and to counterbalance the bending energy of the surfactant in the vesicle phase. For this reason, the stable phase is vesicular and not flat lamellar, as found at lower pH values.

In the *MLWV* phase, between pH 7.5 and 4, the *d*-spacing of the lamellar wall progressively increases from $d = 34.9 \text{ \AA}$ ($q_l = 0.180 \text{ \AA}^{-1}$) to $d = 40.2 \text{ \AA}$ ($q_l = 0.156 \text{ \AA}^{-1}$), before precipitation of the *L* phase below pH 4 with $d = 34.8 \text{ \AA}$ ($q = 0.181 \text{ \AA}^{-1}$) measured at pH 3 (Figure 5d). At the moment of formation, *MLWV* have the same *d*-spacing value as in the *L* phase and this value is less than 1 \AA shorter compared to the lamellar period in the G-C18:1 *L* phase control ($d = 35.7 \text{ \AA}$). The fact that the shortest *d*-spacing in the *MLWV* is comparable to the control is counterintuitive, because the interlamellar volume in the *MLWV* must accommodate PLL chains, which occupy a given volume. However, from the theory of polyelectrolyte adsorption on surfaces of opposite charges and from many experimental works, it is well-known that polyelectrolytes can form a flat 2D layer.^{71,74} In this case, the thickness of the polyelectrolyte layer corresponds to its molecular cross-section. The cross-sectional diameter of PLL is reasonably expected to be contained between 1 \AA and 8 \AA , the former being the lower limit found in many polymeric systems⁷⁵ and the latter estimated in bilayer/PLL multilayers at pH below 7.⁷⁶ The thickness of the G-C18:1 interdigitated layer can be calculated to be 32.8 \AA by applying the Tanford formula ($L = 1.54 + 1.265 \cdot n$, *L* being the length of the aliphatic chain and *n* the number of methylene groups)⁶⁷ to an effective C16 aliphatic chain (considering the 120° of the double bond in G-C18:1) and taking 8 \AA as the size of a single glucose molecule.⁷⁷ Experimentally, we have estimated the thickness of the G-C18:1 membrane to be contained between 28 \AA (pH 7) and 30 \AA (pH 6) by modelling SAXS data (Figure S 4 in Ref. ⁴⁶), with an error due to fitting process of at least $\pm 10 \%$. To account for the experimental *d*-spacing values, one has to consider a hydration interlamellar layer between 5.7 and 7.7 \AA in the PLL-free control system, which can be classically found in lipid lamellar phases.^{78,79} At the moment of formation of the *MLWV* at pH 7 ($d = 34.9 \text{ \AA}$), one can otherwise estimate the contribution of PLL to the interlamellar layer to be contained between 4.9 \AA and 6.9 \AA , the latter being in better agreement with what it was experimentally reported in ref. ⁷⁶ and taking into account a thickness of the IL of 28 \AA .

Several points should be highlighted from the above:

- Considering the thickness of the lipid membrane, the resulting interlamellar space is compatible with the diameter of PLL. In other words, a single PLL layer accommodates in

between G-C18:1 interdigitated layers during the formation of *MLWV* in agreement with the dilute and semidilute regimes described in ref. ⁷¹.

- Considering the fact that the interlamellar distance is practically equivalent to the expected diameter of PLL, one does not expect a significant content of hydration water and counterions in the proximity of PLL. This is consistent with the entropic gain of releasing water molecule and counterions during the formation of PESCs.^{4,24} However, hydration water and counterions can fill the space between adjacent polyelectrolyte molecules, as also implied by the semidilute regimes described in ref. ⁷¹.

- At the moment of *MLWV* formation and after precipitation of the *L* phase below pH 4, the thickness of the interlamellar space is the same and it is comparable with the interlamellar thickness in the PLL-free control. This fact shows that PLL can partly replace hydration water, confirming the assumptions above.

- Considering that *d*-spacing is the same at the moment of *MLWV* formation at pH 7 and after precipitation of the *L* phase below pH 4, one could formulate the hypothesis that PLL is trapped in the *L* phase. Our data cannot directly prove this assumption, but we will provide more insights on this point in the following paragraphs, suggesting that this is not the case.

- Increase of the *d*-spacing in the *MLWV* between pH 7 and pH 4 is certainly related to the protonation of G-C18:1, an analogous, although opposite, mechanism described for systems composed of lipid membrane with constant charge density and pH-reactive polyelectrolytes.²⁰ A more detailed explanation of the pH-dependent evolution profiles of both *d*-spacing and size of lamellar crystallites (Figure 5d) is given below.

- Reversibility of the *Co*-to-*MLWV* to *MLWV*-to-*Co* phase transitions is addressed on Figure S 10, of which a)-panel focuses on the alkaline-to-acidic *Co*-to-*MLWV* transition ($C = 10 \text{ mg mL}^{-1}$), discussed above, and b)-panel highlights the reversed acidic-to-alkaline pH variation performed on the same sample. Figure S 10b shows the lamellar peak of the *Co*-to-*MLWV* phase but it does not show any evidence of the correlation peak typical of the *Co* phase, indicating that the *Co*-to-*MLWV* phase transition is not reversible. This is probably due to the screening effect of salt generated during the pH variation process and known to have a strong impact on the phase diagram.²⁴

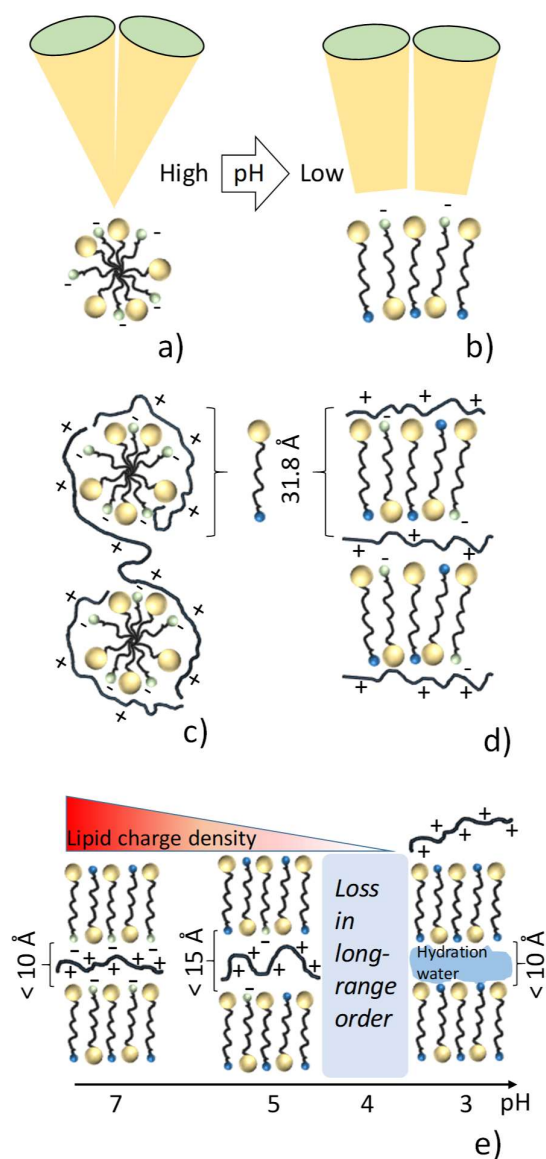


Figure 6 – Schematic view of the pH-driven transition between (a) micelles and (b) interdigitated membrane composed solely of G-C18:1. In the presence of PLL, the transition between the (a) complex coacervate and (b) the multi-lamellar wall in the *MLWV* occurs via a morphology change (micelle-to-vesicle) but a structural continuity (micelle-diameter \approx membrane thickness). e) Insight on the evolution of the pH-dependent interlamellar spacing inside the multi-lamellar walls of *MLWV*: upon decrease in the membrane charge density, PLL expands and it applies a repulsive pressure to the lipid membranes. When the membrane is close to neutrality, long-range order is lost, *MLWV* disassembles, PLL is expelled and G-C18:1 precipitates into a hydrated lamellar phase.

The pH-dependent d -spacing evolution is explained by looking at the intermolecular forces equilibrating in the interlamellar space. In a polymer-free lipid bilayer system, attractive Van der Waals interaction counterbalances two short-range (< 30 Å), steric and hydration, and

two long-range ($> 30 \text{ \AA}$ up to hundred of nanometers) repulsive interactions, electrostatic and thermal undulation.^{80–82} For interlamellar spacing below 30 \AA , which is the case here, electrostatic and undulation are generally neglected. In the case of a polyelectrolyte contained between membranes with variable charge density, which is the case in this work, one should consider additional terms in the energy balance like a repulsive free polymer term, including chain elasticity and excluded-volume terms, an entropic contribution of the small ions, an electrostatic contribution, containing the polyelectrolyte-surface attractive and inter-chain repulsive interaction.^{37,38,70,71,83,84} Under the conditions of *MLWV* formation, around pH 7, the negatively-charged G-C18:1 membrane undergoes strong electrostatic attraction with PLL, largely-documented in both theoretical and experimental works on polyelectrolytes at charged interfaces.^{38,70,71,84–86} When pH decreases, the carboxylate to carboxylic acid reaction reduces the number of negative charges and, consequently, it lowers the charge density of the lipid membrane. Since the attractive electrostatic component in the lipid-polyelectrolyte complex depends on the lipid charge density, lowering pH will reduce its contribution to the free energy. The consequence will be an increased volume occupied by the polyelectrolyte,⁷¹ which will cause an increase in the repulsive osmotic pressure^{37,38} with consequent swelling of the membranes, experimentally shown in Figure 5b,d and schematized in Figure 6e.

Below pH 4, the *MLWV* peak disappears until pH ~ 3 , when the signal of the *L* phase at $d = 34.8 \text{ \AA}$ appears again. Interestingly, this value is practically the same one observed at the moment of the *MLWV* formation at pH 7 and actually 0.9 \AA smaller than the d -spacing found in the G-C18:1 control at the same pH value. Such an observation could induce to formulate the hypothesis that in the *MLWV*-to-*L* phase transition below pH 4, PLL is confined in between the lamellae. In fact, we believe that this is not the case for several reasons. It is well-known that at low hydration and in the absence of specific attraction interactions, large polymers segregate outside the lipid interlamellar space.⁸⁷ However, the polymer cannot be reasonably expelled from a dense, closed, multilamellar object. The evolution of the crystallite size with pH in Figure 5d helps understanding the mechanism of expulsion. Between pH 5 and 4, d -spacing is still increasing, testifying of the expansion of the lamellae due to the repulsive pressure applied by PLL. In the meanwhile, the peak becomes larger, with consequent drop in the crystallite size. At pH 4, the peak becomes so large that the crystallite size has dropped from several thousand of Ångstrom to only few Ångstrom, while d -spacing drops back to 34.7 \AA . Below pH 5, the repulsive pressure exerted by PLL becomes so strong that the long-range order in the *MLWV* is lost. Complete disruption of the multilamellar walls occurs below pH 4, when PLL could eventually be expelled in the surrounding aqueous solution. Upon expulsion of PLL,

G-C18:1 precipitates in its thermodynamically favorable *L* phase, the same as found in the control lipid solution. This mechanism is summarized in Figure 6e at pH below 5.

Discussion

Figure 7 summarizes the major findings of this work. SL-C18:0 is a lipid which undergoes a direct micelle-to-fiber transition in water in the vicinity of pH 7. We had proposed a nucleation and growth mechanism of the fibers with no apparent structural continuity with the micelles, which act as reservoir of matter.^{46,56} In the presence of a polyelectrolyte, such mechanism persists. Above pH 7.5, the negatively-charged micelles are complexed by the polyelectrolyte into a complex coacervate phase, of which we found two major structures by cryo-TEM, a dense cluster of micelles coexisting with a more textured pattern (Figure 4a). Below pH 7.5, the coacervate phase disassembles in favour of a twisted ribbon phase, presumably composed of SL-C18:0 only and surrounded by free polyelectrolyte aqueous solution. Interestingly, ribbons composed of bile salt were proposed to interact with block copolymers after fibrillation,⁴³ and for this reason we speculate that SL-C18:0 fibers are neutral objects. As in the PEC-free system, the coacervate-to-fiber transition occurs in less than a pH unit and without any intermediate. This general mechanism is shown in Figure 7a. The best hypothesis, to be eventually verified with other complementary techniques, is that upon charge compensation during lowering pH, SL-C18:0 molecules are progressively acidified and slowly diffuse from the micellar environment to the solution. The solubility of acidic SL-C18:0 in water is low and for this reason, after reaching a critical concentration, nucleation of the twisted ribbons occurs, followed by growth and concomitant disruption of the coacervate. Last but not least, the nature of the PEC has no influence on the coacervate-to-fiber transition, indicating that PEC rigidity and charge density play no significant role.

G-C18:1 undergoes a micelle-to-vesicle-to-lamellar phase transition, characterized by a structural and morphological continuity.⁴⁶ In the presence of PLL (generalization to other PEC will be presented elsewhere),⁶¹ G-C18:1 forms a complex coacervate phase in the micelle region of its phase diagram at pH > 7. Combination of cryo-TEM and SAXS suggests a textured worm-like structure of the coacervate (Figure 4b). Below approximately pH 7.5, we find a transition between the complex coacervate and multilamellar walls vesicles. This is driven by an isostructural and isodimensional (Figure 6c,d) micelle-to-membrane transition (Figure 6a,b): the diameter of the micelles, embedded in the coacervate phase, is equivalent to the thickness of the membrane. The thickness corresponds to the length of a single G-C18:1 molecule (Figure 6d), as previously found for this systems⁴⁶ and expected for bolaamphiphiles.⁶⁸ *MLWV* are stable in the pH interval between 7 and 5. A decrease in pH corresponds to an increasing content

of the acidic form of G-C18:1 in the membrane and a consequent lowering of the membrane charge density. For this reason, the interlamellar distance increases by decreasing pH, due to the increasing thickness of PLL, hence causing an increase in repulsive pressure, upon lowering the charge density of the membrane (Figure 6e).⁷¹ When the amount of negative charges has lowered at a point below which attractive interaction with PLL can no longer hold the membranes together (between pH 5 and pH 4), *MLWV* experience a loss in the long-range lamellar order. This is followed by the complete disruption of the *MLWV*, causing the expulsion of PLL and eventually followed, below pH 3, by precipitation of a polyelectrolyte-free lamellar phase only composed of G-C18:1 (Figure 6e and Figure 7b). If pH is increased again, *MLWV* form again in their pH stability range. However, further increase in pH does not induce a reversed *MLWV*-to-*Co* transition, but rather the formation of free micelles and PLL.

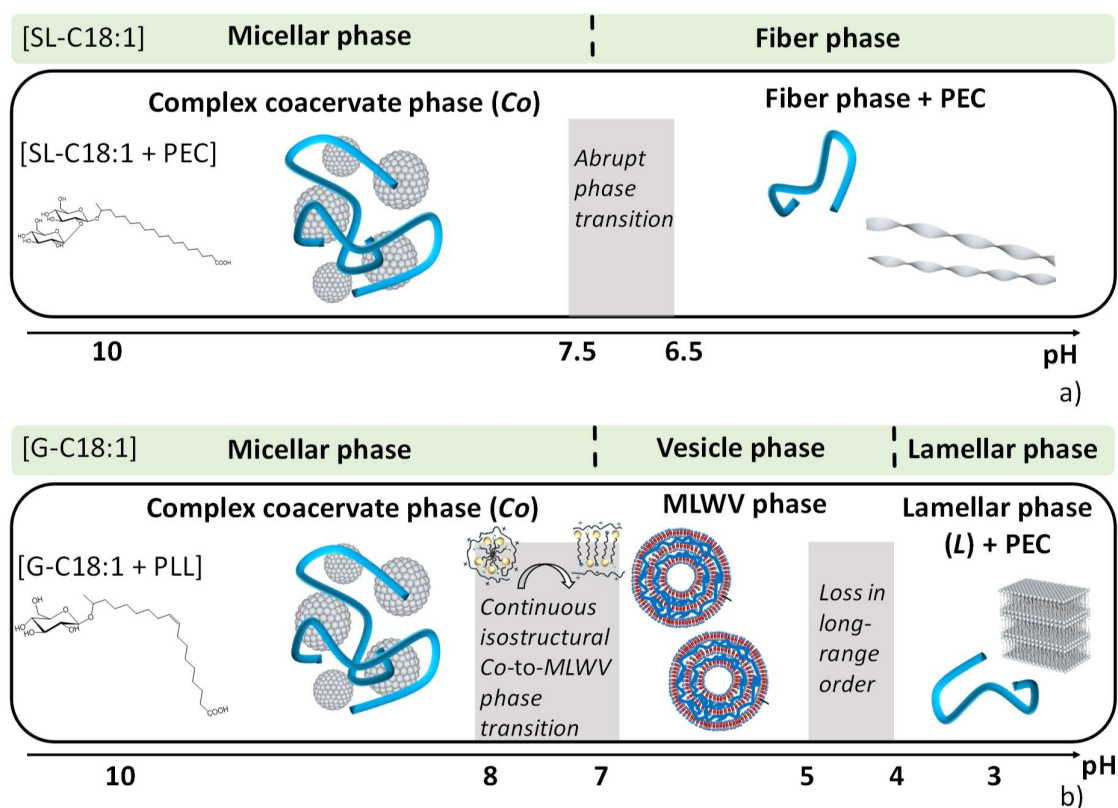


Figure 7 – Summary of the pH-driven phase transitions of (a) SL-C18:0 and (b) G-C18:1 lipids alone and in the presence of PLL polyelectrolyte in water at room temperature and $C < 1$ wt%.

Our data show that the *Co*-to-*MLWV* is driven by the dynamic variation in the effective packing parameter of G-C18:1 and which depends on the transition from its ionic to neutral form. If this result is coherent with previous studies on the equilibrium phase diagrams of

PECSs, where the packing parameter of the PESC was modified either by using a cosurfactant^{6,23} or by varying the nature of the polar headgroup,³² we do not find a major influence of the type of polyelectrolyte, as proposed elsewhere.⁷ This is unexpected, especially considering the strong impact of polyelectrolytes on the membrane bending energy already discussed above. It has been recently shown that the pH-driven micelle-to-vesicle transition in free ethoxy fatty acids solutions³¹ can be inhibited in the presence of a polyelectrolyte.³² In fact, to the best of our knowledge, evidence of isostructural and isodimensional micelle-to-vesicle transition in PESCs at concentrations as low as 0.2 wt% have hardly been described. Lamellar or multilamellar PESCs phases are far from being uncommon but they are generally obtained for calibrated formulations³² and often at high lipid concentrations (generally above 10 wt%).²³ Furthermore, similar phase transitions were never reported in specific polyelectrolyte-surfactant complex coacervate systems.

It is worth mentioning a short comment on the *MLWV* structure, which we systematically find, instead of flat lamellar phase or agglutinated single-wall vesicles. We have discussed the former situation as the overwhelming effect of the intrinsic bending energy of the G-C18:1 interdigitated layered membrane overwhelming the competing structuring effect of the polyelectrolyte. Although we cannot quantify it, it seems clear that none of the polyelectrolytes employed in this study are neither rigid enough nor bind strongly enough to generate a flat membrane.

Whether the non-equilibrium continuous pH variation to cross the micelle-vesicle boundary of G-C18:1 has any impact on the *Co*-to-*MLWV* transition is an open question to which we can answer only partially. Vesicles are generally considered as metastable structures, although in some cases, when the structure does not evolve for an “infinitely” long time, they are assumed to be at equilibrium. G-C18:1 spontaneously self-assembles into vesicles upon pH variation from alkaline to acidic pH under conditions of both pseudo-⁵¹ and non-equilibrium (Figure 5a).⁴⁶ Furthermore, unpublished in-lab tests show that G-C18:1 in fact spontaneously forms vesicles by a simple dispersion in water at pH below 7 and by application of moderate amounts of energy (e.g., bath sonication). G-C18:1 vesicles tend to be colloiddally stable over long periods of time (months). On the basis of these observation, one can qualitatively say that the vesicle phase is the thermodynamic phase of G-C18:1 under acidic pH conditions. Given the above, *MLWV* structures should be systematically obtained if pH is varied extremely slow or if a G-C18:1 pre-formed vesicles and PEC solutions are mixed at acidic pH. In the first approach, it would be hard and ridiculously long to determine which rate of pH variation would be considered to be compatible with equilibrium conditions. For instance, Chiappisi *et al.* have

employed equilibration times for a given pH value between 2 and 15 days.^{32,65} For this reason, we have employed the second approach, reported elsewhere,⁶¹ and which does not show the formation of a single MLWV phase but rather a multiphasic system composed of agglutinated vesicles, cabbage-like structure and MLWV.

Agglutination of single-wall vesicles (SWV)^{24,88,89} against the formation of *MLWV* is an open, and important, question in the literature both from a fundamental⁸⁹ and applicative points of view, as agglutination is important in the field of life science,⁸⁹ while *MLWV* have a specific interest in gene transfection applications.⁹⁰ If several authors have explained the origin of *MLWV* structures as a simple matter of lipid-to-polyelectrolyte ratio,^{3,90,91} other authors show contradictory data, where a mixture of both can be found.⁹² In the present system, we rather believe that the systematic production of *MLWV*, instead of agglutinated SWV, depends on the combination between the pre-existing complex coacervate phase, inside which the isostructural and isodimensional micelle-to-vesicle phase transition occurs, and the non-equilibrium pH variation, which traps the system in the MLWV phase. Separation between these mechanisms should be studied in more depth in future works.

Conclusion

Non-equilibrium phase transitions in polyelectrolyte-surfactant complex (PESC) coacervates (*Co*) are addressed in this work by mean of stimuli-responsive negatively-charged amphiphiles and cationic polyelectrolytes. We employ two microbial glycolipid biosurfactants known to undergo micelle-to-fiber (deacetylated acidic C18:0 sophorolipids, SL-C18:0) and micelle-to-vesicle (deacetylated acidic C18:1 glucolipids, G-C18:1) phase transition when pH is lowered from alkaline to acidic. In the alkaline pH domain, both amphiphiles mainly form a phase characterized by negatively-charged micelles. Upon mixing with a positively-charged polyelectrolyte, pH-resolved *in situ* SAXS, DLS and ζ -potential combined with cryo-TEM show the formation of globally neutral PESC polyelectrolyte-surfactant coacervates. Upon acidification of the solution, the SL-C18:0 amphiphile undergoes a micelle-to-fiber transition, independently from the presence of the polyelectrolyte, which is most likely released in solution and it coexists with the fibers, but without specific interactions, differently than other similar systems.⁴³ The micelle-to-fiber transition is hence responsible for the disruption of the complex coacervate, which becomes unstable below pH ~ 7 , the transition pH of the SL-C18:0 surfactant alone.

At the micelle-vesicle boundary, we find a continuous isostructural and isodimensional transition between complex coacervate (*Co*) and multilamellar wall vesicles (*MLWV*). By

reducing the negative charge density during acidification, the micellar aggregates embedded in the *Co* phase are characterized by a decrease in the local curvature, which drives the transition from spheres to membranes, composed of interdigitated G-C18:1 molecules. The residual negative charge density guarantees electrostatic interaction with the polyelectrolyte, which keeps the membranes together. The bending energy associated to the polyelectrolyte-membrane complex is low enough for the lipid membrane to bend and drive the formation of vesicular colloids, characterized by multilamellar walls. The membrane thickness is equivalent to the micellar radius and compatible with the length of G-C18:1, testifying the isostructural and isodimensional transition. At lower pH, the membrane charge density becomes low and interactions with the polyelectrolyte less strong. This phenomenon promotes intra-chain electrostatic repulsion interactions and eventual swelling of the lamellar region. Finally, when the membrane becomes neutral, polymeric repulsion becomes strong enough to disassemble the lamellae. The polyelectrolyte will most likely be entirely solvated and at sufficiently low pH (< 3) the G-C18:1 precipitated in the form of a poorly-ordered, polyelectrolyte-free, lamellar phase, as found in the control lipid solution at the same pH. Upon increasing pH, *MLWV* form again but we do not find reversibility in the *MLWV*-to-*Co* transition.

This work shows that surfactant phase transitions driven by a non-equilibrium pH variation drive the complex coacervate out of its stability region. This occurs either through the loss of the polyelectrolyte-surfactant aggregation or through the formation of a new complex phase. In both cases, the nature of the polyelectrolyte (e.g., rigidity or charge density) does not have any significant influence on the fate of the transition, as found for most PESC. For the *MLWV* phase, the bending energy of the lipid membrane is low enough to counterbalance the strong adsorption and stiffness of the polyelectrolyte, which could otherwise drive the formation of a flat lamellar phase. At the same time, combination between the isostructural and isodimensional transition occurring in the confined micellar complex coacervate with non-equilibrium pH variation drive the formation of a *MLWV* phase, interesting for biomedical applications, rather than of a system composed of agglutinated single-wall vesicles, as found in many other systems. Finally, we stress the fact that this work demonstrates the possibility to prepare a new generation of stimuli-responsive and fully sustainable PESC due to the use of biosurfactants.

Acknowledgements

Diamond synchrotron radiation facility (U. K.) is acknowledged for accessing to the B21 beamline and financial support (proposal N° 23247). Ghazi Ben Messaoud (DWI-Leibniz Institute for Interactive Materials, Aachen, Germany) is kindly acknowledged for helpful discussions. We thank Dr. S. Roelants, Prof. W. Soetaert and Prof. C. V. Stevens at Gent University for providing us the glycolipids. This work benefited from the use of the SasView application, originally developed under NSF award DMR-0520547. SasView contains code developed with funding from the European Union's Horizon 2020 research and innovation program under the SINE2020 project, grant agreement No. 654000

Supporting Information: Figure S1 to Figure S10, explicative text.

References

- (1) Kronberg, B.; Holmberg, K.; Lindman, B. *Surface Chemistry of Surfactants and Polymers*; John Wiley & Sons, Inc., 2014.
- (2) *Dna Interactions With Polymers and Surfactants*; Dias, R., Lindman, B., Eds.; John Wiley & Sons, Inc.: Hoboken, New Jersey, 2008.
- (3) Gradzielski, M.; Hoffmann, I. Polyelectrolyte-Surfactant Complexes (PESCs) Composed of Oppositely Charged Components. *Curr. Opin. Colloid Interface Sci.* **2018**, *35*, 124–141.
- (4) Ferreira, G. A.; Loh, W. Liquid Crystalline Nanoparticles Formed by Oppositely Charged Surfactant-Polyelectrolyte Complexes. *Curr. Opin. Colloid Interface Sci.* **2017**, *32*, 11–22.
- (5) Lindman, B.; Antunes, F.; Aidarova, S.; Miguel, M.; Nylander, T. Polyelectrolyte-Surfactant Association—from Fundamentals to Applications. *Colloid J.* **2014**, *76*, 585–594.
- (6) Piculell, L. Understanding and Exploiting the Phase Behavior of Mixtures of Oppositely Charged Polymers and Surfactants in Water. *Langmuir* **2013**, *29*, 10313–10329.
- (7) Chiappisi, L.; Hoffmann, I.; Gradzielski, M. Complexes of Oppositely Charged Polyelectrolytes and Surfactants - Recent Developments in the Field of Biologically Derived Polyelectrolytes. *Soft Matter* **2013**, *9*, 3896–3909.
- (8) Schmitt, C.; Turgeon, S. L. Protein/Polysaccharide Complexes and Coacervates in Food Systems. *Adv. Colloid Interface Sci.* **2011**, *167*, 63–70.
- (9) Winslow, B. D.; Shao, H.; Stewart, R. J.; Tresco, P. A. Biocompatibility of Adhesive

- Complex Coacervates Modeled after the Sandcastle Glue of *Phragmatopoma Californica* for Craniofacial Reconstruction. *Biomaterials* **2010**, *31*, 9373–9381.
- (10) Johnson, N. R.; Wang, Y. Coacervate Delivery Systems for Proteins and Small Molecule Drugs. *Expert Opin. Drug Deliv.* **2014**, *11*, 1829–1832.
 - (11) Hwang, D. S.; Zeng, H.; Srivastava, A.; Krogstad, D. V.; Tirrell, M.; Israelachvili, J. N.; Waite, J. H. Viscosity and Interfacial Properties in a Mussel-Inspired Adhesive Coacervate. *Soft Matter* **2010**, *6*, 3232–3236.
 - (12) Baccile, N.; Reboul, J.; Blanc, B.; Coq, B.; Lacroix-Desmazes, P.; In, M.; Gérardin, C. Ecodesign of Ordered Mesoporous Materials Obtained with Switchable Micellar Assemblies. *Angew. Chemie - Int. Ed.* **2008**, *47*, 8433–8437.
 - (13) Chiappisi, L.; Simon, M.; Gradzielski, M. Toward Bioderived Intelligent Nanocarriers for Controlled Pollutant Recovery and PH-Sensitive Binding. *ACS Appl. Mater. Interfaces* **2015**, *7*, 6139–6145.
 - (14) Hiwatari, Y.; Yoshida, K.; Akutsu, T.; Yabu, M.; Iwai, S. Polyelectrolyte-Micelle Coacervation: Effect of Coacervate on the Properties of Shampoo. *J. Soc. Cosmet. Chem. Japan* **2004**, *26*, 315–316.
 - (15) Burgess, D. J.; Ponsart, S. B-Glucuronidase Activity Following Complex Coacervation and Spray Drying Microencapsulation. *J. Microencapsul.* **1998**, *15*, 569–579.
 - (16) Wang, Y. F.; Gao, J. Y.; Dubin, P. L. Protein Separation via Polyelectrolyte Coacervation: Selectivity and Efficiency. *Biotechnol. Prog.* **1996**, *12*, 356–362.
 - (17) Jones, O. G.; Lesmes, U.; Dubin, P.; McClements, D. J. Effect of Polysaccharide Charge on Formation and Properties of Biopolymer Nanoparticles Created by Heat Treatment of β -Lactoglobulin-Pectin Complexes. *Food Hydrocoll.* **2010**, *24*, 374–383.
 - (18) Israelachvili, J. N.; Mitchell, D. J.; Ninham, B. W. Theory of Self-Assembly of Hydrocarbon Amphiphiles into Micelles and Bilayers. *J. Chem. Soc. Faraday Trans. 2* **1976**, *72*, 1525.
 - (19) Bilalov, A.; Olsson, U.; Lindman, B. Complexation between DNA and Surfactants and Lipids: Phase Behavior and Molecular Organization. *Soft Matter* **2012**, *8*, 11022–11033.
 - (20) Kogej, K. Association and Structure Formation in Oppositely Charged Polyelectrolyte-Surfactant Mixtures. *Adv. Colloid Interface Sci.* **2010**, *158*, 68–83.
 - (21) Kizilay, E.; Kayitmazer, A. B.; Dubin, P. L. Complexation and Coacervation of Polyelectrolytes with Oppositely Charged Colloids. *Adv. Colloid Interface Sci.* **2011**, *167*, 24–37.

- (22) Kizilay, E.; Dinsmore, A. D.; Hoagland, D. A.; Sun, L.; Dubin, P. L. Evolution of Hierarchical Structures in Polyelectrolyte-Micelle Coacervates. *Soft Matter* **2013**, *9*, 7320–7332.
- (23) Piculell, L.; Norrman, J.; Svensson, A. V.; Lynch, I.; Bernardes, J. S.; Loh, W. Ionic Surfactants with Polymeric Counterions. *Adv. Colloid Interface Sci.* **2009**, *147–148*, 228–236.
- (24) Antunes, F. E.; Marques, E. F.; Miguel, M. G.; Lindman, B. Polymer-Vesicle Association. *Adv. Colloid Interface Sci.* **2009**, *147–148*, 18–35.
- (25) Stanic, V.; Mancuso, M.; Wong, W.; Dimasi, E.; Strey, H. H. Phase Diagrams of Electrostatically Self-Assembled Amphiplexes. *Macromolecules* **2011**, *44*, 7423–7429.
- (26) Mekhloufi, G.; Sanchez, C.; Renard, D.; Guillemin, S.; Hardy, J. PH-Induced Structural Transitions during Complexation and Coacervation of β -Lactoglobulin and Acacia Gum. *Langmuir* **2005**, *21*, 386–394.
- (27) Rawat, K.; Aswal, V. K.; Bohidar, H. B. DNA-Gelatin Complex Coacervation, UCST and First-Order Phase Transition of Coacervate to Anisotropic Ion Gel in 1-Methyl-3-Octylimidazolium Chloride Ionic Liquid Solutions. *J. Phys. Chem. B* **2012**, *116*, 14805–14816.
- (28) Vieregg, J. R.; Lueckheide, M.; Marciel, A. B.; Leon, L.; Bologna, A. J.; Rivera, J. R.; Tirrell, M. V. Oligonucleotide-Peptide Complexes: Phase Control by Hybridization. *J. Am. Chem. Soc.* **2018**, *140*, 1632–1638.
- (29) Lasic, D. D. *Liposomes: From Physics to Applications*; Elsevier, Ed.; 1993.
- (30) Leng, J.; Egelhaaf, S. U.; Cates, M. E. Kinetics of the Micelle-to-Vesicle Transition: Aqueous Lecithin-Bile Salt Mixtures. *Biophys. J. Vol.* **2003**, *85*, 1624–1646.
- (31) Hayward, D. W.; Chiappisi, L.; Teo, J. H.; Prévost, S.; Schweins, R.; Gradzielski, M. Neutralisation Rate Controls the Self-Assembly of PH-Sensitive Surfactants. *Soft Matter* **2019**, *15*, 8611–8620.
- (32) Chiappisi, L.; Prévost, S.; Grillo, I.; Gradzielski, M. From Crab Shells to Smart Systems: Chitosan-Alkylethoxy Carboxylate Complexes. *Langmuir* **2014**, *30*, 10615–10616.
- (33) Brooks, J. T.; Marques, C. M.; Cates, M. E. The Effect of Adsorbed Polymer on the Elastic Moduli of Surfactant Bilayers. *J. Phys. II* **1991**, *1*, 673–690.
- (34) Harries, D.; Ben-Shaul, A.; Szleifer, I. Enveloping of Charged Proteins by Lipid Bilayers. *J. Phys. Chem. B* **2004**, *108*, 1491–1496.
- (35) May, S.; Ben-Shaul, A. DNA-Lipid Complexes: Stability of Honeycomb-like and

- Spaghetti-like Structures. *Biophys. J.* **1997**, *73*, 2427–2440.
- (36) May, S. Stability of Macroion-Decorated Lipid Membranes. *J. Phys. Condens. Matter* **2005**, *17*.
- (37) Sjöström, L.; Åkesson, T.; Jönsson, B. Interaction and Conformation of Polyelectrolyte Chains Adsorbed on Neutral Surfaces. *J. Chem. Phys.* **1993**, *99*, 4739–4747.
- (38) Fleer, G. J.; Stuart, M. A. C.; Scheutjens, J. M. H. M.; Cosgrove, T.; Vincent, B. *Polymers at Interfaces*, 1998th ed.; Springer-Science, 1998.
- (39) Wang, J.; Guo, K.; Qiu, F.; Zhang, H.; Yang, Y. Predicting Shapes of Polymer-Chain-Anchored Fluid Vesicles. *Phys. Rev. E - Stat. Nonlinear, Soft Matter Phys.* **2005**, *71*, 1–5.
- (40) Li, D.; Wagner, N. J. Universal Binding Behavior for Ionic Alkyl Surfactants with Oppositely Charged Polyelectrolytes. *J. Am. Chem. Soc.* **2013**, *135*, 17547–17555.
- (41) Okesola, B. O.; Smith, D. K. Applying Low-Molecular Weight Supramolecular Gelators in an Environmental Setting-Self-Assembled Gels as Smart Materials for Pollutant Removal. *Chem. Soc. Rev.* **2016**, *45*, 4226–4251.
- (42) Liu, X. Y.; Sawant, P. D. Formation Kinetics of Fractal Nanofiber Networks in Organogels. *Appl. Phys. Lett.* **2001**, *79*, 3518–3520.
- (43) Di Gregorio, M. C.; Gubitosi, M.; Travaglini, L.; Pavel, N. V.; Jover, A.; Meijide, F.; Vázquez Tato, J.; Sennato, S.; Schillén, K.; Tranchini, F.; et al. Supramolecular Assembly of a Thermoresponsive Steroidal Surfactant with an Oppositely Charged Thermoresponsive Block Copolymer. *Phys. Chem. Chem. Phys.* **2017**, *19*, 1504–1515.
- (44) Dhasaiyan, P.; Prasad, B. L. V. Self-Assembly of Bolaamphiphilic Molecules. *Chem. Rec.* **2017**, *17*, 597–610.
- (45) Kitamoto, D.; Morita, T.; Fukuoka, T.; Konishi, M.; Imura, T. Self-Assembling Properties of Glycolipid Biosurfactants and Their Potential Applications. *Curr. Op. Coll. Interf. Sci.* **2009**, *14*, 315–328.
- (46) Baccile, N.; Cuvier, A.-S.; Prévost, S.; Stevens, C. V.; Delbeke, E.; Berton, J.; Soetaert, W.; Van Bogaert, I. N. A.; Roelants, S. Self-Assembly Mechanism of PH-Responsive Glycolipids: Micelles, Fibers, Vesicles, and Bilayers. *Langmuir* **2016**, *32*, 10881–10894.
- (47) Palareti, G.; Legnani, C.; Cosmi, B.; Antonucci, E.; Erba, N.; Poli, D.; Testa, S.; Toso, A. Comparison between Different D-Dimer Cutoff Values to Assess the Individual Risk of Recurrent Venous Thromboembolism: Analysis of Results Obtained in the DULCIS Study. *Int. J. Lab. Hematol.* **2016**, *38*, 42–49.

- (48) Baccile, N.; Pedersen, J. S.; Pehau-Arnaudet, G.; Van Bogaert, I. N. a. Surface Charge of Acidic Sophorolipid Micelles: Effect of Base and Time. *Soft Matter* **2013**, *9*, 4911–4922.
- (49) Baccile, N.; Babonneau, F.; Jestin, J.; Pehau-Arnaudet, G.; Van Bogaert, I. Unusual, PH-Induced, Self-Assembly of Sophorolipid Biosurfactants. *ACS Nano* **2012**, *6*, 4763–4776.
- (50) Ben Messaoud, G.; Promeneur, L.; Brennich, M.; Roelants, S. L. K. W.; Le Griel, P.; Baccile, N. Complex Coacervation of Natural Sophorolipid Bolaamphiphile Micelles with Cationic Polyelectrolytes. *Green Chem.* **2018**, *20*, 3371–3385.
- (51) Baccile, N.; Selmane, M.; Le Griel, P.; Prévost, S.; Perez, J.; Stevens, C. V.; Delbeke, E.; Zibek, S.; Guenther, M.; Soetaert, W.; et al. PH-Driven Self-Assembly of Acidic Microbial Glycolipids. *Langmuir* **2016**.
- (52) Cuvier, A. S.; Berton, J.; Stevens, C. V.; Fadda, G. C.; Babonneau, F.; Van Bogaert, I. N. A.; Soetaert, W.; Pehau-Arnaudet, G.; Baccile, N. PH-Triggered Formation of Nanoribbons from Yeast-Derived Glycolipid Biosurfactants. *Soft Matter* **2014**, *10*, 3950–3959.
- (53) Liu, W.; Sun, S.; Cao, Z.; Zhang, X.; Yao, K.; Lu, W. W.; Luk, K. D. K. An Investigation on the Physicochemical Properties of Chitosan/DNA Polyelectrolyte Complexes. *Biomaterials* **2005**, *26*, 2705–2711.
- (54) Lewis, S. R.; Datta, S.; Gui, M.; Coker, E. L.; Huggins, F. E.; Daunert, S.; Bachas, L.; Bhattacharyya, D. Reactive Nanostructured Membranes for Water Purification. *Proc. Natl. Acad. Sci. U. S. A.* **2011**, *108*, 8577–8582.
- (55) Mady, M. M.; Mohammed, W. A.; El-Guendy, N. M.; Elsayed, A. A. Effect of Polymer Molecular Weight on the Dna/Pei Polyplexes Properties. *J. Biophys* **2011**, *21*, 151–165.
- (56) Ben Messaoud, G.; Le Griel, P.; Hermida-Merino, D.; Roelants, S. L. K. W.; Soetaert, W.; Stevens, C. V.; Baccile, N. PH-Controlled Self-Assembled Fibrillar Network (SAFiN) Hydrogels: Evidence of a Kinetic Control of the Mechanical Properties. *Chem. Mater.* **2019**, *31*, 4817–4830.
- (57) Schindelin, J.; Arganda-Carreras, I.; Frise, E.; Kaynig, V.; Longair, M.; Pietzsch, T.; Preibisch, S.; Rueden, C.; Saalfeld, S.; Schmid, B.; et al. Fiji: An Open-Source Platform for Biological-Image Analysis. *Nat. Methods* **2012**, *9*, 676–682.
- (58) Koga, S.; Williams, D. S.; Perriman, A. W.; Mann, S. Peptide-Nucleotide Microdroplets as a Step towards a Membrane-Free Protocell Model. *Nat. Chem.* **2011**,

3, 720–724.

- (59) Swanson-Vethamuthu, M.; Dubin, P. L.; Almgren, M.; Yingjie, L. Cryo-TEM of Polyelectrolyte – Micelle Complexes. *J. Colloid Interface Sci.* **1997**, *186*, 414–419.
- (60) Rinaudo, M. Chitin and Chitosan: Properties and Applications. *Prog. Polym. Sci.* **2006**, *31*, 603–632.
- (61) Seyrig, C.; Griel, P. Le; Cowieson, N.; Perez, J.; Baccile, N. Synthesis of Multilamellar Walls Vesicles (MLWV) Polyelectrolyte Surfactant Complexes (PESCs) from PH-Stimulated Phase Transition Using Microbial Biosurfactants. *ChemRxiv* **2020**, 10.26434/chemrxiv.12058929.
- (62) Xu, A. Y.; Melton, L. D.; Ryan, T. M.; Mata, J. P.; Rekas, A.; Williams, M. A. K.; McGillivray, D. J. Effects of Polysaccharide Charge Pattern on the Microstructures of β -Lactoglobulin-Pectin Complex Coacervates, Studied by SAXS and SANS. *Food Hydrocoll.* **2018**, *77*, 952–963.
- (63) Kronberg, B.; Holmberg, K.; Lindman, B. Surfactant–Polymer Systems. In *Surface Chemistry of Surfactants and Polymers*; Kronberg, B., Holmberg, K., Lindman, B., Eds.; John Wiley & Sons, Ltd., 2014; pp 271–294.
- (64) Dias, R. S.; Dawson, K.; Miguel, M. G. Interaction of DNA with Surfactants in Solution. In *DNA Interactions with Polymers and Surfactants*; Dias, R., Lindman, B., Eds.; Hoboken, New Jersey, 2008; pp 89–117.
- (65) Chiappisi, L.; David Leach, S.; Gradzielski, M. Precipitating Polyelectrolyte-Surfactant Systems by Admixing a Nonionic Surfactant-a Case of Cononsurfactancy. *Soft Matter* **2017**, *13*, 4988–4996.
- (66) Israelachvili, J. N.; Mitchell, D. J. A Model for the Packing of Lipids in Bilayer Membranes. *Biochim. Biophys. Acta* **1975**, *389*, 13–19.
- (67) Tanford, C. *The Hydrophobic Effect: Formation of Micelles and Biological Membranes*; Wiley-Interscience, 1973.
- (68) Nagarajan, R. Self-Assembly of Bola Amphiphiles. *Chem. Eng. Commun.* **1987**, *55*, 251–273.
- (69) Manet, S.; Cuvier, A. S.; Valotteau, C.; Fadda, G. C.; Perez, J.; Karakas, E.; Abel, S.; Baccile, N. Structure of Bolaamphiphile Sophorolipid Micelles Characterized with SAXS, SANS, and MD Simulations. *J. Phys. Chem. B* **2015**, *119*, 13113–13133.
- (70) Borukhov, I.; Andelman, D.; Orland, H. Polyelectrolyte Solutions between Charged Surfaces. *Europhys. Lett.* **1995**, *32*, 499–504.
- (71) Dobrynin, A. V.; Rubinstein, M. Theory of Polyelectrolytes in Solutions and at

- Surfaces. *Prog. Polym. Sci.* **2005**, *30*, 1049–1118.
- (72) Dan, N.; Pincus, P.; Safran, S. A. Membrane-Induced Interactions between Inclusions. *Langmuir* **1993**, *9*, 2768–2771.
- (73) Winterhalter, M.; Helfrich, W. Effect of Surface Charge on the Curvature Elasticity of Membranes. *J. Phys. Chem* **1988**, *92*, 6865–6867.
- (74) Zinchenko, A. A.; Pyshkina, O. A.; Lezov, A. V.; Sergeyev, V. G.; Yoshikawa, K. Single DNA Molecules: Compaction and Decompaction. In *DNA Interactions with Polymers and Surfactants*; Dias, R., Lindman, B., Eds.; John Wiley & Sons, Inc.: Hoboken, New Jersey, 2008; pp 59–88.
- (75) He, T. Estimating Cross-sectional Area of a Polymer Chain by Additive Method. *J. Appl. Polym. Sci.* **1986**, *31*, 1521–1524.
- (76) Heath, G. R.; Li, M.; Polignano, I. L.; Richens, J. L.; Catucci, G.; O'Shea, P.; Sadeghi, S. J.; Gilardi, G.; Butt, J. N.; Jeuken, L. J. C. Layer-by-Layer Assembly of Supported Lipid Bilayer Poly-L-Lysine Multilayers. *Biomacromolecules* **2016**, *17*, 324–335.
- (77) Netrabukkana, R.; Lourvanij, K.; Rorrer, G. L. Diffusion of Glucose and Glucitol in Microporous and Mesoporous Silicate/Aluminosilicate Catalysts. *Ind. Eng. Chem. Res.* **1996**, *35*, 458–464.
- (78) Parsegian, V. A.; Zemb, T. Hydration Forces: Observations, Explanations, Expectations, Questions. *Curr. Opin. Colloid Interface Sci.* **2011**, *16*, 618–624.
- (79) Leikin, S.; Parsegian, V. A.; Rau, D. C.; Rand, R. P. Hydration Forces. *Annu. Rev. Phys. Chem.* **1993**, *44*, 369–395.
- (80) Dubois, M.; Zemb, T.; Fuller, N.; Rand, R. P.; Parsegian, V. A. Equation of State of a Charged Bilayer System: Measure of the Entropy of the Lamellar-Lamellar Transition in DDABr. *J. Chem. Phys.* **1998**, *108*, 7855–7869.
- (81) Ricoul, F.; Dubois, M.; Belloni, L.; Zemb, T.; André-Barrès, C.; Rico-Lattes, I. Phase Equilibria and Equation of State of a Mixed Cationic Surfactant-Glycolipid Lamellar System. *Langmuir* **1998**, *14*, 2645–2655.
- (82) Leneveu, D. M.; Rand, R. P.; Parsegian, V. A. Measurement of Forces between Lecithin Bilayers. *Nature* **1976**, *259*, 601–603.
- (83) Claesson, P. M. Interactions Between Surfaces Coated with Carbohydrates, Glycolipids, and Glycoproteins. In *Biopolymers at Interfaces, Second Edition*; Malmsten, M., Ed.; CRC Press, 2003; p 165.
- (84) Chatellier, X.; Joanny, J.-F. Adsorption of Polyelectrolyte Solutions on Surfaces: A Debye-Hueckel Theory. *J. Phys. II Fr.* **1996**, *6*, 1669–1686.

- (85) Yethiraj, A. Forces between Surfaces Immersed in Polyelectrolyte Solutions. *J. Chem. Phys.* **1999**, *111*, 1797–1800.
- (86) Dobrynin, A. V.; Deshkovski, A.; Rubinstein, M. Adsorption of Polyelectrolytes on Oppositely Charged Surfaces. *Macromolecules* **2001**, *34*, 3421–3436.
- (87) Rand, R. P.; Parsegian, V. A. Hydration Forces between Phospholipid Bilayers. *BBA - Rev. Biomembr.* **1989**, *988*, 351–376.
- (88) Marques, E. F.; Regev, O.; Khan, A.; Miguel, M. D. G.; Lindman, B. Interactions between Catanionic Vesicles and Oppositely Charged Polyelectrolytes - Phase Behavior and Phase Structure. *Macromolecules* **1999**, *32*, 6626–6637.
- (89) De Souza, T. P.; Bossa, G. V.; Stano, P.; Steiniger, F.; May, S.; Luisi, P. L.; Fahr, A. Vesicle Aggregates as a Model for Primitive Cellular Assemblies. *Phys. Chem. Chem. Phys.* **2017**, *19*, 20082–20092.
- (90) Weisman, S.; Hirsch-Lerner, D.; Barenholz, Y.; Talmon, Y. Nanostructure of Cationic Lipid-Oligonucleotide Complexes. *Biophys. J.* **2004**, *87*, 609–614.
- (91) Ram-On, M.; Cohen, Y.; Talmon, Y. Effect of Polyelectrolyte Stiffness and Solution PH on the Nanostructure of Complexes Formed by Cationic Amphiphiles and Negatively Charged Polyelectrolytes. *J. Phys. Chem. B* **2016**, *120*, 5907–5915.
- (92) Gasperini, A. A. M.; Puentes-Martinez, X. E.; Balbino, T. A.; De Paula Rigoletto, T.; De Sá Cavalcanti Corrêa, G.; Cassago, A.; Portugal, R. V.; De La Torre, L. G.; Cavalcanti, L. P. Association between Cationic Liposomes and Low Molecular Weight Hyaluronic Acid. *Langmuir* **2015**, *31*, 3308–3317.
- (93) Cuvier, A. S.; Babonneau, F.; Berton, J.; Stevens, C. V.; Fadda, G. C.; Péhau-Arnaudet, G.; Le Griel, P.; Prévost, S.; Perez, J.; Baccile, N. Nanoscale Platelet Formation by Monounsaturated and Saturated Sphorolipids under Basic PH Conditions. *Chem. - A Eur. J.* **2015**, *21*, 19265–19277.
- (94) Wang, Y.; Kimura, K.; Huang, Q.; Dubin, P. L. Effects of Salt on Poly Electrolyte-Micelle Coacervation. *Macromolecules* **1999**, *32*, 7128–7134.

Supporting Information

Stimuli-induced non-equilibrium phase transitions polyelectrolyte-surfactant complex coacervates

Chloé Seyrig,^a Patrick Le Griel,^a N. Cowieson,^b Niki Baccile^a

^a Sorbonne Université, Centre National de la Recherche Scientifique, Laboratoire de Chimie de la Matière Condensée de Paris , LCMCP, F-75005 Paris, France

^b Diamond Light Source Ltd, Harwell Science and Innovation Campus, Didcot, OX11 0QX, U.K.

Content: Figure S1 to Figure S10, explicative text

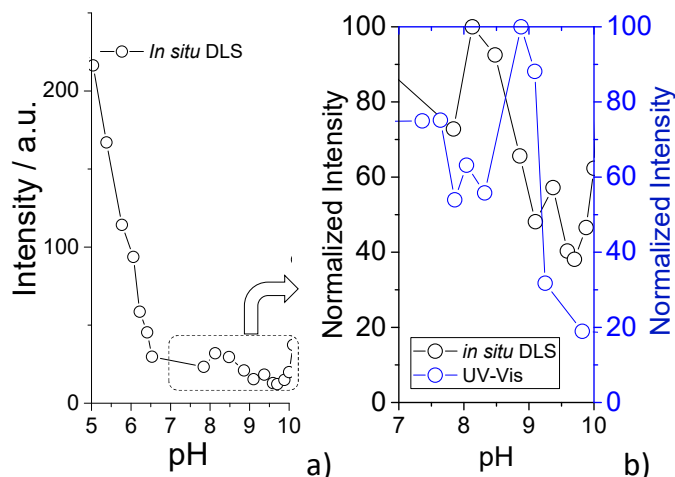


Figure S 1 – a) pH-resolved *in situ* DLS experiment performed on a [SL-C18:0 + PLL] solution at $C_{\text{SL-C18:0}}=2.5 \text{ mg}\cdot\text{mL}^{-1}$ $C_{\text{PLL}}= 2.5 \text{ mg}\cdot\text{mL}^{-1}$. b)-panel shows the normalized intensity recorded using pH-resolved *in situ* DLS and UV-Vis data

To avoid sedimentation issues in the SL-C18:0 fibrillar system, we have repeated the turbidimetric titration of the [SL-C18:0 + PLL] mixture using a continuous flow-through device installed on a light scattering instrument and which guarantees a better homogenization of the sample solution. Data in Figure S 1 show a scattering behavior, in which one can identify some scattering above pH 10, due to the formation of platelets in the SL-C18:0 system alone,⁹³ and a strong scattering below pH 7, as reported elsewhere for the SL-C18:0 system alone.⁵² Interestingly, the region between pH 7 and 10 is characterized by a mild scattering but comparable, after normalization, to the scattering observed in UV-Vis experiments (Figure S 1b). Whichever the method of analysis employed, we systematically find a region of pH, generally between 7 and 10, in which the lipid-PEC mixed solution becomes turbid, differently than the controls.

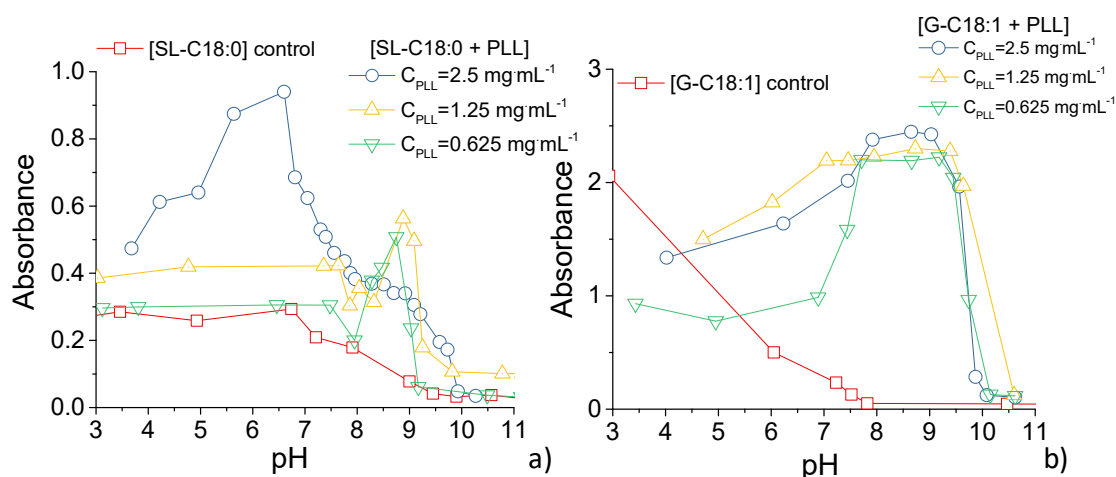


Figure S 2 - Room temperature turbidimetric analysis of a) SL-C18:0 and b) G-C18:1 glycolipid solutions with different concentrations of PLL as a function of pH. The typical sample preparation is described in the materials and method section. The final lipid and PLL concentrations are $C_{\text{G-C18:1}} = C_{\text{SL-C18:0}} = 2.5 \text{ mg mL}^{-1}$, $C_{\text{PLL}} = 2.5, 1.25 \text{ or } 0.625 \text{ mg mL}^{-1}$. pH is decreased from 11 to 3.

The red square curve Figure S 2 refers to the control lipid solutions, displaying a similar behavior: the micellar region at alkaline pH shows poor scattering, while the intensity increases at acidic pH, when SL-C18:0 and G-C18:1 respectively self-assemble into fibers and vesicles. When mixed with different concentrations of PLL, all scattering profiles show a common bell-like shape, with an enhanced signal between pH 7 and 10. Indeed, blue, yellow and green curves, respectively standing for concentration of PLL of 2.5 mg mL^{-1} , 1.25 mg mL^{-1} and 0.625 mg mL^{-1} , show an intensity peak at around pH ~ 8.5 -9. This behavior clearly identifies a preferred pH range of interaction between lipids and PPL, precisely from pH 7 to pH 9.

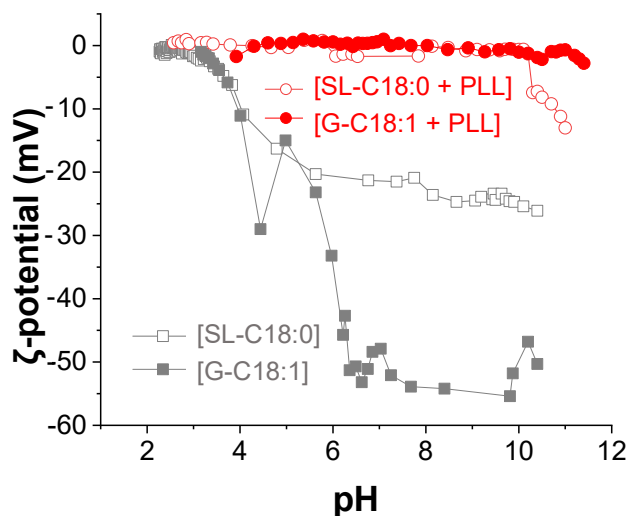


Figure S 3 – ζ -potential measurements of: [SL-C18:0] and [G-C18:1] controls (grey curves); [SL-C18:0 + PLL] and [G-C18:1 + PLL] solutions (red curves) $C_{G-C18:1} = C_{SL-C18:0} = 2.5 \text{ mg mL}^{-1}$, $C_{PLL} = 2.5 \text{ mg mL}^{-1}$

ζ -potential experiments shown in Figure S 3 show that control lipid solutions have the same behavior: they are strongly negative (SL-C18:0 and G-C18:1 respectively show a plateau at -20 mV and -55 mV) under alkaline conditions, but their ζ -potentials slightly increase around pH 6 to finally be close to zero, putting in evidence the neutralization of the carboxylate group. When lipids are mixed with PLL, the resulting curve oscillates around neutral ζ -potential, and charges are perfectly compensated in the pH region of interest, from pH 7 to 9, an argument in favor of coacervation, a process likely occurring in electroneutralization conditions ⁹⁴

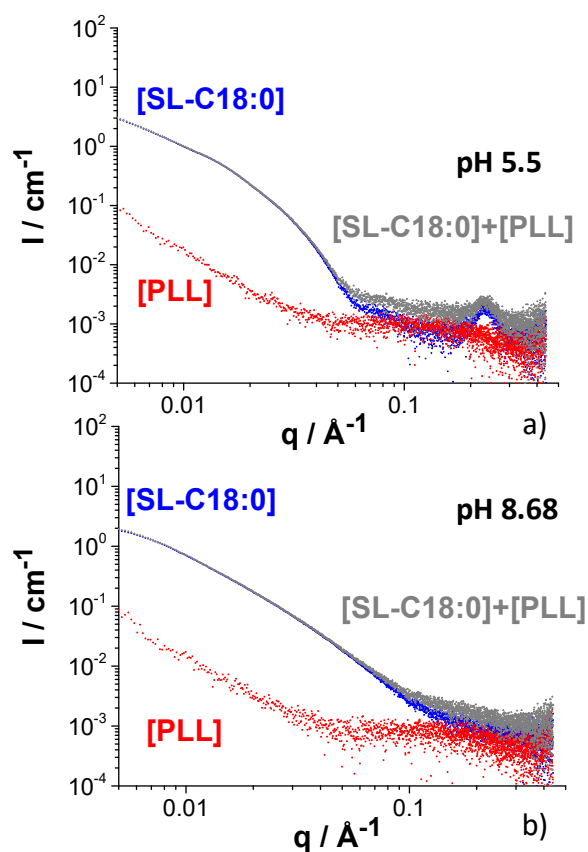


Figure S 4 - SAXS profiles of [SL-C18:0] and [PLL] controls at acidic and basic pH. $C_{\text{SL-C18:0}} = 2.5 \text{ mg}\cdot\text{mL}^{-1}$, $C_{\text{PLL}} = 2.5 \text{ mg}\cdot\text{mL}^{-1}$. [SL-C18:0] + [PLL] refers to the arithmetic sum of individual [SL-C18:0] and [PLL] signals.

Figure S 4 shows the control signals of single components: the red curve for [PLL] alone and the blue one for [SL-C18:0] alone. The grey curve corresponds to the simple arithmetic sum of both signals.

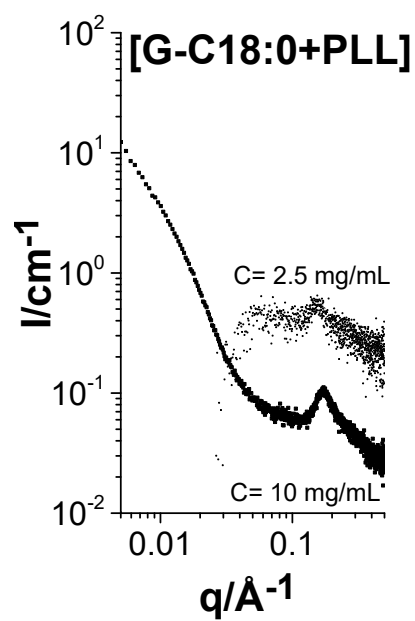


Figure S 5 - SAXS profiles of $[\text{G-C18:1} + \text{PLL}]$ solutions at two concentrations ($C_{\text{G-C18:1}} = C_{\text{PLL}}$) and pH 8.

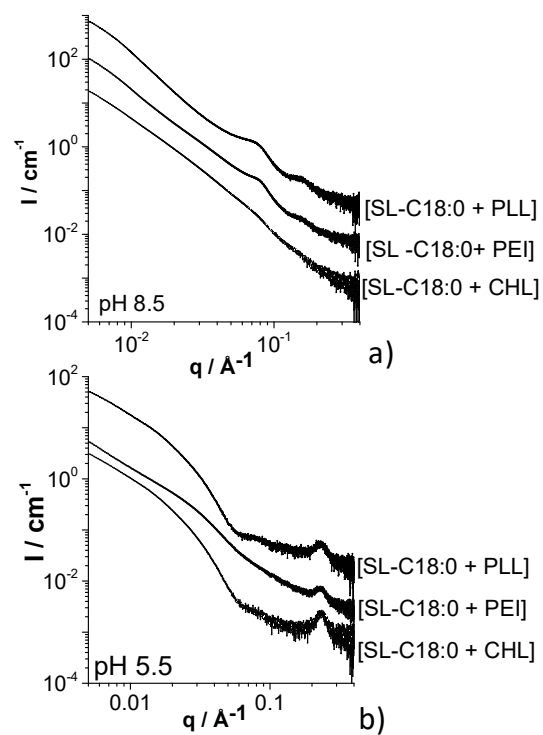


Figure S 6 - SAXS profiles of SL-C18:0 mixed with different polyelectrolytes at acidic and basic pH. $C_{\text{SL-C18:0}} = C_{\text{PLL}} = C_{\text{PEI}} = C_{\text{CHL}} = 2.5 \text{ mg mL}^{-1}$

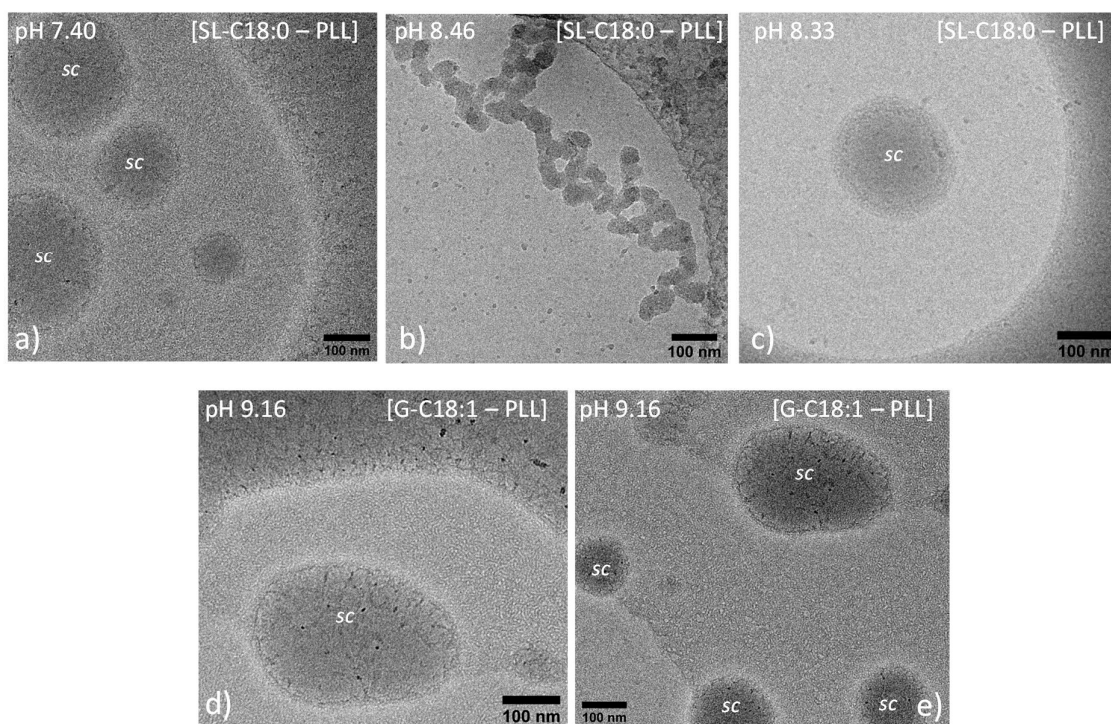


Figure S 7 - Cryo-TEM images of [SL-C18:0 + PLL] and [G-C18:1 + PLL] complex coacervates recorded at various pH values. $C_{\text{SL-C18:0}} = C_{\text{GC-18:1}} = 2.5 \text{ mg mL}^{-1}$; $C_{\text{PLL}} = 1.25 \text{ mg mL}^{-1}$. sc stands for spherical colloid.

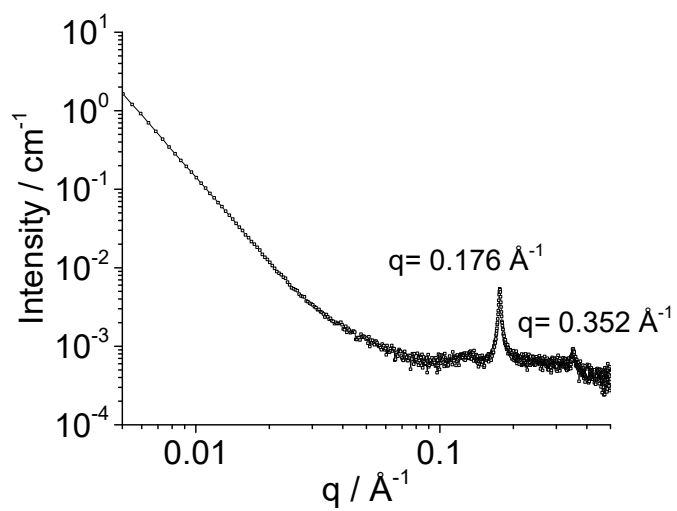


Figure S 8 - SAXS plots of the G-C18:1 control solution at $C=2.5 \text{ mg mL}^{-1}$ and pH 3. Experiment extracted from 2D contour plot in Figure 5a in the main text.

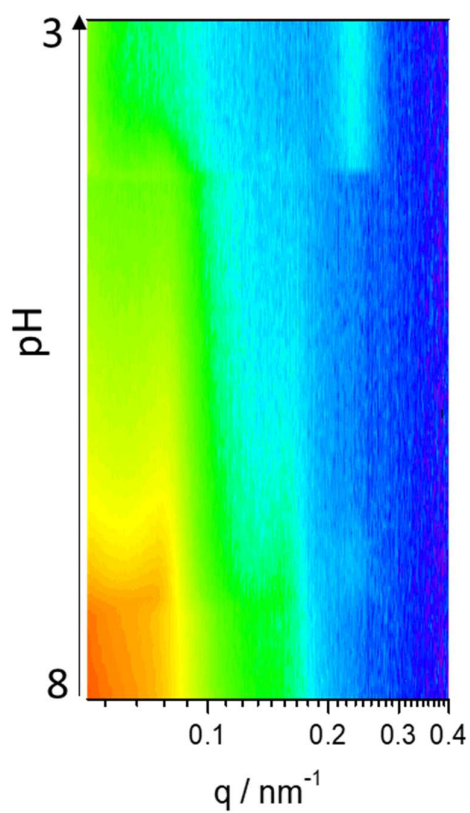


Figure S 9 - pH-resolved *in situ* SAXS 2D contour plot of the [SL-C18:0 + PLL] solution at $C_{\text{SL-C18:0}} = C_{\text{PLL}} = 2.5 \text{ mg}\cdot\text{mL}^{-1}$. Highlight of the coacervate-to-fiber transition between pH 8 and 3.

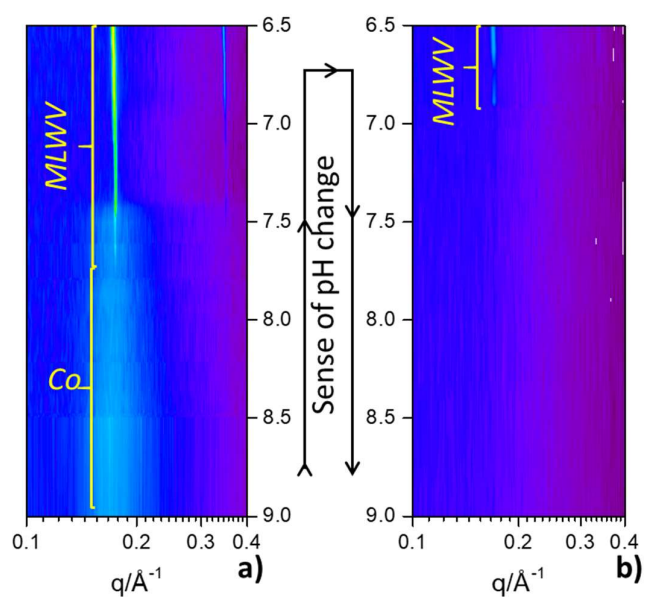


Figure S 10 - pH-resolved *in situ* SAXS 2D contour plots of the [G-C18:1 + PLL] solutions at $C_{G-C18:1} = C_{PLL} = 2.5 \text{ mg}\cdot\text{mL}^{-1}$: highlight of the *Co*-to-*MLWV* transition between pH 9 and 6.5. In a), pH is reduced from 10 to 3. Contour plot in b) is recorded on the same sample as in a), to which pH is increased from 3 to 10.